

This is an Open Access document downloaded from ORCA, Cardiff University's institutional repository: <https://orca.cardiff.ac.uk/id/eprint/149235/>

This is the author's version of a work that was submitted to / accepted for publication.

Citation for final published version:

Brock, Stefanie, Laquerriere, Annie, Marguet, Florent, Myers, Scott J., Hongjie, Yuan, Baralle, Diana, Vanderhasselt, Tim, Stouffs, Katrien, Keymolen, Kathelijm, Kim, Sukhan, Allen, James, Shaulsky, Gil, Chelly, Jamel, Marcorelle, Pascale, Aziza, Jacqueline, Villard, Laurent, Sacaze, Elise, de Wit, Marie C. Y., Wilke, Martina, Mancini, Grazia Maria Simonetta, Hehr, Ute, Lim, Derek, Mansour, Sahar, Traynelis, Stephen F., Beneteau, Claire, Denis-Musquer, Marie, Jansen, Anna C., Fry, Andrew E. and Bahi-Buisson, Nadia 2023. Overlapping cortical malformations in patients with pathogenic variants in GRIN1 and GRIN2B. *Journal of Medical Genetics* 60 (2) , pp. 183-192. 10.1136/jmedgenet-2021-107971

Publishers page: <http://dx.doi.org/10.1136/jmedgenet-2021-107971>

Please note:

Changes made as a result of publishing processes such as copy-editing, formatting and page numbers may not be reflected in this version. For the definitive version of this publication, please refer to the published source. You are advised to consult the publisher's version if you wish to cite this paper.

This version is being made available in accordance with publisher policies. See <http://orca.cf.ac.uk/policies.html> for usage policies. Copyright and moral rights for publications made available in ORCA are retained by the copyright holders.



Overlapping cortical malformations in patients with pathogenic variants in *GRIN1* and *GRIN2B*

Stefanie Brock, MD, ^{1,2}, Annie Laquerrière, MD, PhD, ^{3,4} Florent Marguet, MD, PhD, ^{3,4} Scott J. Myers, PhD ^{5,6}, Hongjie Yuan, MD, PhD ^{5,6} , Diana Baralle, MD, MBBS ⁷ Tim Vanderhasselt, MD, ⁸ Katrien Stouffs, MD, PhD, ^{2,9} Kathelijn Keymolen, MD, PhD, ⁹ Sukhan Kim,^{5,6} , James P. Allen ^{5,6}, Gil Shaulsky ^{5,6}, Jamel Chelly, MD, PhD, ^{10,11} Pascale Marcorelles, MD, PhD, ¹² Jacqueline Aziza, MD, ¹³ Laurent Villard, PhD, ^{14, 15} Elise Sacaze, MSc, ¹⁶ Marie Claire de Wit, MD, PhD, ¹⁷ Martina Wilke, MD,¹⁸ Grazia Mancini, MD, PhD, ¹⁸ Ute Hehr, MD, ¹⁹ Derek Lim, MBChB, ²⁰ Sahar Mansour, BMBS, FRCP, ²¹ , Stephen F. Traynelis, PhD, ^{5,6} Claire Beneteau, MD, ^{22, 23}, Marie Denis-Musquer, MD, ^{23, 24} Anna C. Jansen, MD, PhD, ^{2,25} Andrew E. Fry, MBChB, DPhil, ^{26, 27*} and Nadia Bahi-Buisson, MD, PhD, ^{28,29*}

1. Universitair Ziekenhuis Brussel (UZ Brussel), Department of Pathology, Laarbeeklaan 101, 1090 Brussels, Belgium
2. Neurogenetics Research Group, Reproduction Genetics and Regenerative Medicine Research Cluster, Vrije Universiteit Brussel (VUB), Laarbeeklaan 101, 1090 Brussels, Belgium
3. Normandie Univ, UNIROUEN, Inserm U1245, Normandy Centre for Genomic and Personalized Medicine, F 76000, Rouen, France
4. Rouen University Hospital, Department of Pathology, F 76000, Rouen, France
5. Department of Pharmacology and Chemical Biology, Emory University School of Medicine, Atlanta, GA, USA

6. Center for Functional Evaluation of Rare Variants (CFERV), Emory University
School of Medicine, Atlanta, GA, USA
7. Human Development and Health, Faculty of Medicine, University of Southampton.
8. Universitair Ziekenhuis Brussel (UZ Brussel), Department of Radiology,
Laarbeeklaan 101, 1090 Brussels, Belgium
9. Center for Reproduction and Genetics, Universitair Ziekenhuis Brussel (UZ Brussel),
Laarbeeklaan 101, 1090 Brussels, Belgium
10. Institut de Génétique et de Biologie Moléculaire et Cellulaire, CNRS UMR 7104,
INSERM U1258, Université de Strasbourg, 1 rue Laurent Fries, 67404 Illkirch, France
11. Laboratoire de Diagnostic Génétique, Hôpitaux Universitaire de Strasbourg, 67000
Strasbourg, France
12. Department of Pathology, Brest University Hospital, France
13. Department of Pathology, University Institute for Cancer, 32059 Toulouse, France
14. Aix Marseille Univ, Inserm, Marseille Medical Genetics Center, Marseille, France
15. Department of Medical Genetics, La Timone Children's Hospital, Marseille, France
16. Department of Pediatrics, Brest University Hospital, France
17. Department of Pediatric Neurology, ENCORE Expertise Center for
neurodevelopmental disorders, Erasmus MC University Medical Center, Rotterdam,
The Netherlands.
18. Department of Clinical Genetics, Erasmus MC University Medical Center, Rotterdam,
The Netherlands
19. Center for Human Genetics, University of Regensburg, Regensburg, Bayern, 93047
Germany
20. West Midlands Regional Genetics Service and Birmingham Health Partners,
Birmingham Women's and Children's Hospitals NHS Foundation Trust, Birmingham,
UK

21. SW Thames Regional Genetics Service, St. George's University NHS Foundation Trust, London, UK
22. C.H.U Nantes, Department of Genetics, 1 place Alexis Ricordeau, 44093 Nantes, France
23. C.H.U Nantes, UF de Fœtopathologie et Génétique, 1 place Alexis Ricordeau, 44093 Nantes, France
24. C.H.U Nantes, Department of Pathology, 1 place Alexis Ricordeau, 44093 Nantes, France
25. Universitair Ziekenhuis Brussel (UZ Brussel), Pediatric Neurology Unit, Laarbeeklaan 101, 1090 Brussels, Belgium
26. Institute of Medical Genetics, University Hospital of Wales, Cardiff CF14 4XW, UK
27. Division of Cancer and Genetics, School of Medicine, Cardiff University, Cardiff CF14 4XN, UK
28. Université Paris Descartes - Sorbonne Paris Cités, Paris, France
29. Institut Imagine (INSERM UMR-1163), Embryology and genetics of congenital malformations, Paris, France

Correspondence:

Dr Stefanie Brock, Department of Pathology, UZ Brussel, Laarbeeklaan 101, 1090 Brussels, Belgium; E-mail: stefanie.brock@uzbrussel.be, Tel +32(0)24775084

Dr Andrew E. Fry, Institute of Medical Genetics, University Hospital of Wales, Cardiff, CF14 4XW, United Kingdom; E-mail: fryae@cardiff.ac.uk, Tel. +44 (0)29 2074 3151

ABSTRACT

Background: Malformations of cortical development (MCD) have been reported in a subset of patients with pathogenic heterozygous variants in *GRIN1* or *GRIN2B*, genes which encode for subunits of the N-methyl-D-aspartate (NMDA) receptor. The aim of this study was to further define the phenotypic spectrum of NMDAR-related MCDs.

Methods: We report the clinical, radiological, and molecular features of seven new patients and review data on 18 previously reported individuals with NMDAR-related MCDs. Neuropathological findings for two individuals with heterozygous variants in *GRIN1* are presented. We report clinical and neuropathological features of one additional individual with homozygous pathogenic variants in *GRIN1*.

Results: Heterozygous variants in *GRIN1* and *GRIN2B* were associated with overlapping severe clinical and imaging features, including global developmental delay, epilepsy, diffuse dysgyria, dysmorphic basal ganglia and hippocampi. Neuropathological examination in two foetuses with heterozygous *GRIN1* variants suggests that proliferation as well as radial and tangential neuronal migration are impaired. In addition, we show that neuronal migration is also impaired by homozygous *GRIN1* variants in an individual with microcephaly with simplified gyral pattern.

Conclusion: These findings expand our understanding of the clinical and imaging features of the 'NMDARopathy' spectrum and contribute to our understanding of the likely underlying pathogenic mechanisms leading to MCD in these patients.

Keywords: GRIN1, GRIN2B, NMDAR, malformations of cortical development,
polymicrogyria

INTRODUCTION

N-methyl-D-aspartate receptors (NMDARs) are ligand-gated cation channels mediating excitatory synaptic transmission. The NMDAR is a heteromeric complex typically composed of two GluN1 subunits (encoded by *GRIN1*) and two GluN2 subunits (encoded by *GRIN2A-D*). The combination of different subunits influences receptor function.[1, 2] NMDAR subunits contain a discontinuous ligand binding domain (S1 and S2), an intracellular re-entrant pore loop (M2) and three transmembrane domains (M1, M3 and M4).[3] NMDAR subunits exhibit different spatiotemporal expression patterns. The essential glycine-binding GluN1 subunit is highly and ubiquitously expressed in the fetal and adult brain.[2] In contrast, the glutamate-binding subunit GluN2B (encoded by *GRIN2B*) is highly expressed prenatally with progressive limitation to the forebrain, before being replaced postnatally by GluN2A (encoded by *GRIN2A*).[4]

Pathogenic variants in *GRIN1* and *GRIN2B* have been described in individuals with a spectrum of neurological phenotypes. In individuals with heterozygous pathogenic variants, common features include developmental delay, intellectual disability, epilepsy, cortical visual impairment, neurobehavioral problems and movement disorders.[5–10] Homozygous variants have only rarely been reported in *GRIN1*. These include four individuals from two different families with homozygous missense variants, developmental delay, movement disorders but without seizures [9, 11]; and four individuals from two families with homozygous truncating variants with severe neonatal epileptic encephalopathy.[9, 12] Homozygous variants in *GRIN2B* have not been reported yet. To date, 12 patients harbouring *de novo* heterozygous pathogenic variants in *GRIN1* and six patients with pathogenic variants in *GRIN2B* have been reported to have MCDs.[13–15] This subset of patients accounts for approximately 10-15% of all reported individuals with pathogenic variants in either *GRIN1* or *GRIN2B*. [16, 17] Based on radiological appearance, the MCDs observed in patients with pathogenic variants in

GRIN1 or *GRIN2B* are characterized by variable sulcal depth and/or orientation with normal cortical thickness. This was described as ‘dysgyria’, the generic term for abnormal cerebral cortex, although the malformation seems to closely resemble polymicrogyria.[13, 18] However, histopathological evidence has not been available from previous patients to confirm this. Associated brain malformations such as dysmorphic basal ganglia, hypoplastic corpus callosum and hippocampal dysplasia have been reported.[13, 15] The pattern of brain malformations associated with NMDAR-associated MCDs has been noted to resemble that of tubulinopathies.[13, 15]

To provide further insights into the clinical and radiological features of NMDAR-associated MCDs, we report four patients with pathogenic heterozygous variants in *GRIN1* and three patients with heterozygous variants in *GRIN2B* who all presented with complex brain malformations, including dysgyria, and malformations of the hippocampus and basal ganglia. In addition, we present a single patient with a homozygous variant in *GRIN1* associated with a simplified gyral pattern (SGP). The neuropathological data, which were available for two foetuses with *de novo* heterozygous *GRIN1* variants and the neonate with the homozygous *GRIN1* variant, contribute to our understanding of the underlying pathophysiological mechanisms causing the phenotypic features of NMDAR-associated MCD.

MATERIALS AND METHODS

Patient selection

The patients were identified through the Neuro-MIG Network (COST Action CA16118). The study was approved by the ethical committee of the UZ Brussel (B.U.N.143201214360). Three of the patients (individuals 1, 2 and 7) were part of the Deciphering Developmental Disorders (DDD) study.[19] The DDD study was approved by the Cambridge South Research Ethics Committee (10/H0305/83). Clinical data was collected through clinical examination and review of medical records. Imaging data was reviewed by the authors (S.B., A.E.F., N.B-B.).

Genetic analysis

DNA preparation and genetic investigation was undertaken with informed consent from the parents or guardians of the patients. DNA was derived from saliva (individuals 1, 2 and 7), blood (individuals 5, 6 and 8) and by amniocentesis (individuals 3 and 4). DNA was extracted using standard protocols. Whole-exome sequencing (WES) was performed in individuals 1-4, and 6 and 7. Individuals 5 and 8 were tested by next-generation sequencing (NGS) multi-gene panels. Sanger sequencing was used in all individuals except for individual 6 to validate the variants and to test parents. The positions of variants are based on transcripts NM_007327.3 for *GRIN1* and NM_000834.3 for *GRIN2B*. Variants were classified using American College of Medical Genetics and Genomics and Association for Molecular Pathology (ACMG-AMP) criteria.[20, 21]

Electrophysiological analysis

A detailed description of these methods is provided in the Supplementary Material. In summary, the p.Cys744Tyr and the p.Ala653Thr variants were introduced into a plasmid expression construct containing the human GluN1-1a cDNA (hereafter GluN1, based on NM_007327.3) and the p.Met818Thr introduced into human GluN2B cDNA (NM_000834.3) via a QuikChange mutagenesis protocol. The cRNAs for wild type and mutant forms of GluN1, were co-injected with wild-type human GluN2A cRNA and wild-type and mutant forms of GluN2B with wild-type human GluN1 cRNA into *Xenopus laevis* oocytes. The expressed receptors were functionally evaluated by two-electrode voltage clamp (TEVC) recordings for dose response to L-glutamate, glycine, Mg²⁺ and Zn²⁺ ions, and for proton sensitivity.

Neuropathological studies

After complete autopsy, brains were fixed in a 10% formaldehyde-zinc buffer solution. Macroscopic and microscopic examination was performed according to standardized procedures. Immunohistochemical studies were performed using markers for neuronal progenitors, migrating neurons and interneurons as well as for cortical layering (Supplementary material). Results were compared with age-matched controls aged 25, 30 and 39 gestational weeks, respectively.

RESULTS

Clinical features in MCD patients with pathogenic heterozygous variants in *GRIN1* and *GRIN2B*

We identified seven unrelated MCD patients (individuals 1-7) with *de novo* heterozygous pathogenic variants in either *GRIN1* or *GRIN2B*. Clinical findings for individuals 1 to 7 are summarized in Table 1. Two individuals with *GRIN1* variants (individuals 1 and 2) and the three individuals with *GRIN2B* variants presented with microcephaly, severe developmental delay and epilepsy. The age of seizure onset ranged from the neonatal period to 2 years of age. Seizure types were variable, and refractory to treatment in two individuals. Individuals 3 and 4 were foetuses with variants in *GRIN1* that underwent termination of pregnancy. Autopsy and neuropathological findings from individuals 3 and 4 are described in the section below.

In total, 25 MCD patients with heterozygous variants in either *GRIN1* or *GRIN2B* have now been reported in this series and in the wider literature. We reviewed the available clinical information for these 25 patients (Supplementary material, Tables S1 and S2). *GRIN1* or *GRIN2B* MCD patients had overlapping severe clinical phenotypes. Common features in this combined cohort included severe or profound developmental delay or intellectual disability (13/13 in *GRIN1*, 9/9 in *GRIN2B*), epilepsy (13/13 in *GRIN1*, 9/9 in *GRIN2B*), microcephaly (12/14 in *GRIN1*, 5/6 in *GRIN2B*), spastic quadriparesis (9/12 in *GRIN1*, 2/3 in *GRIN2B*) and cortical visual impairment (10/11 in *GRIN1*, 4/5 in *GRIN2B*). Movement disorders were present in 3/5 individuals with variants in *GRIN1* but have not been reported in individuals with variants in *GRIN2B*. The age of onset of epilepsy was variable across this combined cohort ranging from the neonatal period to 1 year for *GRIN1*, and from 10 weeks to 2 years 3 months for *GRIN2B*. Epilepsy phenotypes were also variable in the combined cohort,

including epileptic spasms in 2/12 individuals with variants in *GRIN1* and 5/9 individuals with variants in *GRIN2B*.

Brain imaging in MCD patients with pathogenic variants in *GRIN1* and *GRIN2B*

Brain magnetic resonance imaging (MRI) was performed in all seven individuals with heterozygous variants in *GRIN1* or *GRIN2B* in our series between 29 weeks gestation and three years of age (Table 1, Figure 1), except for individual 3 (in which only prenatal ultrasound was performed). All individuals with variants in *GRIN1* presented with abnormal gyration. The two living *GRIN1* patients (individuals 1 and 2) exhibited bilateral dysgyria, predominantly affecting the frontal regions. Among the *GRIN2B* patients, individuals 5 and 6 demonstrated diffuse bilateral dysgyria while individual 7 had bilateral but asymmetric dysgyria predominantly affecting the left hemisphere.

We reviewed the available neuroradiology for all 25 heterozygous NMDAR MCD patients (Supplementary material, Tables S1 and S2). We found that the MRI phenotypes of *GRIN1*- and *GRIN2B* patients were very similar (Supplementary material, Table S3). Common MRI features in the combined cohort included diffuse bilateral dysgyria often with some posterior sparing, reduced white matter, enlarged lateral ventricles, hippocampal dysplasia, hypoplastic corpus callosum, and enlarged or dysmorphic basal ganglia. The brainstem was normal on imaging in all *GRIN1* and *GRIN2B* patients, except for mildly reduced myelination of the brainstem in individual 1 in this study. The cerebellum was abnormal in 3 individuals with variants in *GRIN1*, but normal in all individuals with variants in *GRIN2B*. It was not possible to distinguish *GRIN1*- and *GRIN2B*-related MCDs based on the radiological findings alone.

Molecular findings in MCD patients with pathogenic variants in *GRIN1* and *GRIN2B*

We identified three *GRIN1* and two *GRIN2B* variants that have not previously been reported. The variants were classified as pathogenic or likely pathogenic (Supplementary material, Tables S4 and S5). The p.(Ser553Leu) *GRIN1* variant in individual 1 is a pathogenic variant previously reported in an unrelated MCD patient.[13] The p.(Met818Thr) *GRIN2B* variant in individual 7 has previously been reported in a non-MCD patient.[15] The seven variants were located in the same regions where previous MCD-associated NMDAR variants have clustered (Figure 2).

To investigate the impact of two *GRIN1* variants and one *GRIN2B* variant, functional studies were performed. The full results are given in the supplementary data section 3. Compared to wild type GluN1 the concentration that elicits a half-maximal current (EC_{50}) for GluN1-C744Y, GluN1-A653T and GluN2B-M818T were reduced for L-glutamate and for glycine, indicating these agonists have significantly greater potency (i.e. produce responses at lower agonist concentrations). Mutant receptors were also less sensitive to inhibition by protons. Expression of the variants GluN1-C744Y and GluN1-A653T subunit protein does not appear to be altered substantially as the expressed levels of both surface and total receptor protein were modest. Overall, these *in vitro* electrophysiological and biochemical analyses suggest that the three variants cause a gain of function.

Table 1. Clinical and imaging features of novel patients with variants in *GRIN1* and *GRIN2B*

Individual	1	2	3	4	5	6	7	8
Gene	GRIN1	GRIN1	GRIN1	GRIN1	GRIN2B	GRIN2B	GRIN2B	GRIN1
Mutation	c.1658C>T, p.(Ser553Leu)	c.1972G>T, p.(Asp658Tyr)	c.1957G>A, p.(Ala653Thr)	c.2231G>A, p.(Cys744Tyr)	c.2437C>G, p.(Leu813Val)	c.2438T>C, p.(Leu813Pro)	c.2453T>C; p.(Met818Thr)	c.1422C>A, p.(Tyr474*)
Inheritance	<i>De novo</i>	<i>De novo</i>	<i>De novo</i>	<i>De novo</i>	<i>De novo</i>	<i>De novo</i>	<i>De novo</i>	Homozygous, inherited
Age at last review	19 m	n/a	25 GW	30 GW	23 m	2.5 y	15 m	6 d
Sex	Male	Male	Male	n/a	Male	Male	Male	Female
DD	Severe	Severe	n/a	n/a	Severe	Severe	Severe	n/a
Age sz onset	Birth/prenatal	4 m	n/a	n/a	4 m	2 y 3 m	10 w	Early postnatal
Sz type	n/a	Absences, drops, tonic extensions	n/a	n/a	Epileptic spasms, tonic sz	GTCS with fever	Infantile spasms, rapid and rolling eye movements	Status epilepticus
Refractory sz	No	Yes	n/a	n/a	Yes	No	No	Yes
Neurology	Hypertonia	Spastic quadriplegia	n/a	n/a	Spastic quadriplegia	Spastic quadriplegia Truncal hypotonia and limb hypertonia, pseudobulbar palsy	Hypertonia	n/a
Dysmorphism	Long palpebral fissures, shallow orbits, overlapping fingers	Thin upper lips, anteverted nares, high frontal hairline, wide nasal bridge	Prominent philtrum, broad nasal bridge, anteverted nostrils	Marked nasal ridge, prominent philtrum, flat facies, camptodactyly	No	No	No	No

OFC	41.5cm (-5.2 SD)	0.4-2nd percentile	Low brain weight, HC - 2SD	Low brain weight	44 cm (-3.2 SD)	44.8 cm (-2.2 SD)	44 cm (9th centile) at 10 months, at 2.5 years 45 cm (-3.96 SD)	Brain weight within normal limits
Dysgyria	Bilateral diffuse (A>P)	Bilateral diffuse (A>P)	Bilateral diffuse	Bilateral diffuse	Bilateral diffuse	Bilateral diffuse (perisylvian and parietal >)	Asymmetric (Left > Right)	Microcephaly with simplified gyral pattern
Other features	Reduced WM, enlarged LV, hypoplastic CC, abnormal myelination in BS, dysmorphic hippocampus	Reduced WM, enlarged LV, hypoplastic CC, dysmorphic BG	Enlarged third ventricle, absent gyration, ACC	Enlarged LV, operculation of sylvian fissure, enlarged subarachnoid spaces	WM reduced occipitally, colpocephaly, hypoplastic CC, enlarged BG	Reduced WM, enlarged LV, dysmorphic hippocampus	Reduced WM, enlarged Left LV, dysmorphic CC and BG	Bilateral symmetric subcortical atrophy with periventricular leukoencephalopathy

Abbreviations: Age, y(ears), m(onths), w(eeks), d(ays); ACC; agenesis of corpus callosum, A>P, anterior more severe than posterior; BG, basal ganglia; BS, brainstem; CC, corpus callosum; GW, gestational weeks; GTCS, generalized tonic-clonic seizures; LV, lateral ventricles; n/a, not applicable; n/k, not known; SD, standard deviations above or below mean; sz, seizures; WM, white matter

Neuropathological findings in *GRINI* patients

Autopsy and neuropathological examination were performed in individuals 3, 4 and 8. Individuals 3 and 4, harboring *de novo* heterozygous variants in *GRINI*, underwent termination of pregnancy at 25 and 30 weeks gestation, respectively, according to the French law, due to severe brain malformations identified on ultrasound imaging. In individual 3, ultrasound (US) examination performed at 23 WG revealed agenesis of the corpus callosum and of the septum pellucidum. Severe deformations of the extremities consisting in bilateral camptodactyly and equinovarus talipes were noted. Based on these findings a medical termination of the pregnancy was proposed and accepted by both parents. In individual 4, US performed at 24 WG identified mild ventricular dilatation. At 26 WG, control US revealed diffuse dysgyria and MRI performed at 29 WG allowed the detection of absent primary fissures and secondary sulci suggestive of lissencephaly. Neither deformities of the limbs nor polyhydramnios were identified. Both individuals showed mild facial particularities consisting of prominent philtrum, broad nasal ridge with anteverted nostrils and flat facies. Macroscopic and histological examination of the thoracic and abdominal cavity was normal in both cases. Both patients had reduced brain weight for gestational age (<<3rd percentile).[22] On external macroscopic brain examination of individual 3, the brain surface appeared smooth with a dimple-shaped Sylvian fissure (Figure 3A and 3B). On sagittal and coronal sections, the ventricles were enlarged and the corpus callosum was absent. Histologically, the thin cortical ribbon had a diffuse festooned-like appearance suggestive of polymicrogyria under a thick and irregular molecular layer containing some immature neuronal heterotopias, and covered by a persistent transient external granular cell layer (Figure 3C). Nodular heterotopias were also noted in the periventricular regions close to the germinative zone of the dorsal telencephalon, to the ganglionic eminences and within the

basal ganglia (Figure 3D). The infratentorial structures were free of lesions. External macroscopic brain examination in individual 4 revealed diffuse polymicrogyria (Figure 3E). The olfactory tracts were absent. The Sylvian fissure was short, vertically oriented and prematurely closed (closure normally occurs between 36 and 38 weeks gestation). The corpus callosum was hypoplastic in its posterior part (Figure 3E). The lateral ventricles were moderately dilated. The hippocampi appeared to be malrotated (Figure 3F). Histologically, the cortical ribbon was replaced by diffuse and poorly laminated polymicrogyria (Figure 3G) covered by a glia limitans which was focally discontinuous with small foci of overmigration. The internal capsule was hypoplastic, the ganglionic eminences had already regressed and the basal ganglia were dysplastic, as were the thalami which were formed by the juxtaposition of nodules. Small confetti-like heterotopic nodules were observed throughout the intermediate zone (Figure 3H). The cerebellar vermis was hypoplastic but the brainstem and the spinal cord were normal.

We compared the clinical and neuropathological findings of individuals 3 and 4 to individual 8 with novel homozygous truncating variants (p.Tyr474*) in *GRIN1* inherited from asymptomatic heterozygous carrier parents. Shortly after birth, individual 8 developed seizures evolving to status epilepticus. The patient died at 6 days of age. Brain imaging was not performed. Individual 8 had microcephaly with a SGP without tertiary sulci on macroscopic examination (Supplementary material, Figure S1). The corpus callosum was hypoplastic. Histologically, multiple foci of neuronal depletion with loss of lamination and abnormal persistence of the external transient granular cell layer in some areas were observed. In the hippocampus, the dentate gyrus was dysmorphic and discontinuous. Small germinolysis pseudo-cysts were observed along the ventricular walls (Supplementary material, Figure S1).

Measurement of the cortical thickness was 1.97 mm, which does not significantly differ from cortical thickness measured on several control cortical plates between 30 and 38 WG (1.70 to

1.90 mm). These data are not in favour of lissencephaly with thin or thick cortex. Full autopsy did not reveal any additional malformations.

Immunohistochemistry revealed less numerous SOX2 and PAX6-positive proliferating radial glial cells in the ventricular and outer subventricular zones of individual 3 than observed in the control brain aged 24-25 WG (Supplementary material, Table S7). MAP2 antibody which immunolabels radially migrating neurons and pyramidal neurons of layers III and V did not allow for identifying any immunoreactive neuron in the micropolygyric cortex of individual 3, these neurons being observed within the periventricular heterotopic nodules (Figure 4A). In individuals 4 and 8, very few MAP2-positive neurons were identified in the cortical plate. These neurons were misoriented, dysmorphic and/or immature (Figure 4B, C and D). CTIP2 and SATB2-positive neurons were either absent or mislocalized (Figure 4E-H). GABAergic interneurons were aberrantly located or almost absent, as were calretininergic interneurons (Figure 4I-L). These findings highly suggest that functional NDMARs are essential for proper radial and tangential migration without which neurons cannot reach their final location.

DISCUSSION

We presented seven new patients and reviewed all previously reported NMDAR MCD patients with *de novo* heterozygous variants in either *GRIN1* or *GRIN2B*. In addition, we provided the first reports of neuropathological findings in two individuals with heterozygous and one individual with homozygous variants in *GRIN1*. Our findings expand the current understanding of the phenotypic spectrum of NMDAR-associated MCD and provide insight into the suspected underlying pathophysiological mechanisms.

For the 25 patients with heterozygous variants in either *GRIN1* or *GRIN2B* that have now been reported in this series and in the wider literature, we found a striking similarity in imaging and phenotypic features. The predominant imaging pattern of MCD in both groups was an extensive diffuse, bilateral dysgyria resembling polymicrogyria. Commonly associated brain malformations in both groups include enlarged ventricles, hippocampal dysplasia, hypoplastic corpus callosum, and enlarged or dysmorphic basal ganglia. Hippocampal dysplasia has been reported on MRI in 5/15 individuals with variants in *GRIN1* and in 5/9 patients with variants in *GRIN2B*. This feature was confirmed by neuropathological examination in individual 4 and in an individual with a homozygous *GRIN1* variant (individual 8) in our series. The hippocampal abnormalities are likely due to the high expression of NMDAR in the hippocampus.[23] Abnormal basal ganglia were found in 6/14 and 8/9 of individuals with variants in *GRIN1* and *GRIN2B*, respectively, likely reflecting the importance of glutaminergic signaling passing through the basal ganglia. Both hippocampal dysplasia and dysmorphic basal ganglia are rare in patients with MCD in general. Individuals with variants in tubulin genes, referred to as tubulinopathies, also show complex brain malformations, including dysgyria and dysmorphic basal ganglia. Rarely, hippocampal hypo- or dysplasia is present, most frequently in patients with variants in *TUBA1A*. [24, 25] Although there appears to be significant overlap of clinical and imaging findings between

tubulinopathies and the spectrum observed in individuals with variants in *GRIN1* or *GRIN2B*, tubulinopathies are often associated with abnormalities of the corpus callosum, brainstem and cerebellar hypo- or dysplasia, possibly due to the role microtubules play in neuronal migration and axon development.[24] In contrast, the cerebellum and brainstem were usually normal in individuals with variants in either *GRIN1* or *GRIN2B*. Prior to genetic testing, variants in *GRIN1* and *GRIN2B* were not suspected based on clinical or imaging features in the individuals presented in this cohort. This might be due to the small number of individuals with NMDAR-related MCD reported previously. During foetal life, the discovery of microcephaly or microlissencephaly with or without corpus callosum agenesis may correspond to a constellation of etiologies, either environmental or genetic and there are no specific signs identified to date which could point to *GRIN1* and *GRIN2B* as candidate genes. The homogeneous imaging spectrum observed in individuals with *GRIN1* and *GRIN2B* - associated MCD, including diffuse dysgyria, dysmorphic basal ganglia and hippocampal dysplasia without any infratentorial lesions may therefore be a potential diagnostic clue and should trigger consideration of pathogenic variants in NMDAR based on imaging findings in the future.

Clinical features included severe or profound developmental delay or intellectual disability, early onset epilepsy, microcephaly, spastic quadriparesis, and cortical visual impairment. Microcephaly was more common in NMDAR-MCD patients than in NMDAR-patients without MCD, and was present in all seven new patients presented here. Overall, 11/13 (84.6%) reported *GRIN1*-MCD and 6/6 of reported *GRIN2B*-MCD patients for which the information is available have microcephaly (ranging from -2.0 to -7.1 SD in *GRIN1* patients). Six out of 23 (26%) of non-MCD patients with *GRIN1* variants reported by Lemke et al. [9] and 7/56 (12.5%) non-MCD patients with *GRIN2B* missense variants reported by Platzer et al.[15] had microcephaly. Hyperkinetic and stereotyped movement disorders that

have been described in patients with and without MCD and variants in NMDAR.[8, 9, 13–15] Interestingly, none of the individuals in our series have been reported to have abnormal movements. However, it is possible that abnormal movements were present but not recognized, limited by limb spasticity, or misdiagnosed as seizures.

We provided the first neuropathological reports of three individuals with variants in *GRINI*. Individuals 3 and 4 were reported with dysgyria resembling polymicrogyria on brain MRI and *de novo* heterozygous pathogenic variants in *GRINI*. Neuropathological examination confirmed polymicrogyria. Both individuals also had extreme microcephaly, nodular heterotopias in the periventricular and intermediate zones, gaps of the glia limitans and overmigration foci in the meninges, arhinencephaly, dysplastic basal ganglia and hippocampi as well as cerebellar hypoplasia. In addition, we provide first evidence that homozygous loss of function (LOF) variants also cause MCD. Neuropathological examination of individual 8 carrying homozygous *GRINI* variants has revealed microcephaly and a SGP associated with defective lamination of the cortex and malrotated hippocampi.

Taken together, the features observed argue for a crucial role of *GRINI* in the morphological organization of the different neuroanatomical structures during fetal life. Immunohistochemical findings also strongly argue for decreased neuron production as well as delayed and inappropriate radial and tangential migration resulting in microcephaly with polymicrogyria or simplified pattern. Noteworthy, using NMDAR RNA interference with *in utero* electroporation in the cortex of rat embryos, Jaing et al.[26] found severely delayed radial migration, with more than 80% of migrating MAP2-positive projection neurons which could not reach the upper layers of the cortical plate and with 30% of the cells remaining located in the intermediate zone. In addition, it has been shown that developmental disruption of NMDA receptors has major effects on interneuron localization leading to inhibitory

network deficits, in so far as ionotropic NMDARs are normally expressed in tangentially migrating interneurons.[27]

It remains uncertain why a subset of patients with NMDAR variants develops severe MCDs. It has already been highlighted that GRIN-variants associated with diffuse dysgyria tend to have gain of function (GOF) effects, as has been shown by functional studies for two variants in *GRIN1* (p.(Ala653Thr) and p.(Cys744Thr)) and one variant in *GRIN2B* (p.Met818Thr) presented here, while many non-MCD variants are hypofunctional.[9, 13] NMDAR variants with GOF effects have also been observed in patients in which no MCDs were reported.[7, 15, 28, 29] These observations raise the possibility that a patient's genetic background or non-genetic events (e.g. viral infection or hypoxic-ischemic injury) may be contributing to the pathogenesis of NMDAR-MCDs. Another explanation can be subtle changes of cortical architecture that might be missed on imaging studies, as has been shown in individual 8 with SGP and homozygous LOF variants. Of note, the homozygous variants in individual 8 were truncating variants. These are likely to cause complete LOF of *GRIN1*, as has been reported in three siblings and one additional individual with a similar clinical course of neonatal epileptic encephalopathy with homozygous truncating variants in *GRIN1*. [9, 12] Homozygous truncating variants causing complete absence of the protein might therefore be at the most severe end of clinical and neuropathological features of LOF variants in *GRIN1*. Thus, the growing evidence for a genotype-phenotype correlation suggests that intrinsic properties of specific NMDAR variants need to be considered as well.[10] An intermediate imaging phenotype with milder or focal dysgyria has not yet been reported, neither for variants in *GRIN1* nor *GRIN2B*, suggesting different mechanisms of pathogenic variants on protein function. Nevertheless, the SGP in individual 8 demonstrates that MCD can also occur in patients with homozygous LOF variants in *GRIN1*. Thus, the hypothesis of an all-or-nothing mechanism, resulting in two patient population with severe MCD and without MCD

is not supported. Finally, the lack of polymicrogyria in the individual with biallelic LOF variants supports the hypothesis that clinical, histological and pathophysiological differences between gain- and loss of function *GRIN*-variants exist.

The seven heterozygous NMDAR variants reported in our series were located in the same regions as previously reported MCD-associated variants. MCD-associated *GRIN1* variants (Figure 1) have clustered in the S1-M1 linker (pre-M1) region, the Lurcher motif in the M3 region, and the S2 domain of GluN1.[13] MCD-associated *GRIN2B* variants have clustered in the M3, S2 and M4 domains of GluN2B.[15] Interestingly, while non-MCD variants in *GRIN1* and *GRIN2B* have been described, no MCD-associated *GRIN1* variants have yet been reported in the GluN1 M4 helix (a region where around half of non-MCD *GRIN1* variants have been located [7, 9]) or the pre-M1 region of GluN2B. This may reflect functional differences between these two domains between GluN1 and GluN2 subunits.

In the patients reported to date, the spectrum of NMDAR variants, including recurrent variants, such as the p.(Ser553Leu) *GRIN1* variant in individual 1, is different from the variants found in non-MCD patients. An exception to this observation has been the recurrent p.(Met818Thr) in *GRIN2B*, located in the GluN2B M4 helix, which has been reported in both an MCD patient (individual 7 in this paper) and a previously reported non-MCD patient.[15] Neuroimaging data from the non-MCD patient has not been available for review. The variable brain phenotype associated with the recurrent p.(Met818Thr) variant may indicate that additional modifiers, such as non-genetic events or genetic background, can influence the outcome.

Electrophysiological analysis of the GluN1 p.Cys744Tyr variant seen in individual 4 with morphologically polymicrogyria confirmed that the p.Cys744Tyr variant causes gain-of-function (GOF) effects. The Cys744 residue forms a disulfide bond with another cysteine in the S2 domain at residue 798.[30] Mutation of either Cys744 or Cys798 to alanine has been

shown to increase the potency of glutamate and reduce proton inhibition.[31] The Cys744-Cys798 disulphide bond has been shown to modulate behavior of NMDAR in response to redox environment.[30, 32] In pathological situations (e.g. following stroke or hypoxia) the brain environment becomes more reductive which favors free thiol over disulphide formation.[30] It has been proposed that the Cys744-Cys798 bond is a ‘molecular oxygen sensor’ in the brain, responding to low pO₂ levels by controlling how much NO can inhibit NMDA function. [30]

There is evidence that disruption of NMDA signaling can influence the proliferation, migration and maturation of neuronal progenitor cells and post-mitotic neurons.[26, 33] A higher prevalence of microcephaly in MCD patients together with increased potency of the NMDAR during electrophysiological studies and reduced neuronal density on histology suggest increased NMDAR signaling leading to excitotoxic cell death may contribute to the increased frequency of microcephaly. This also suggests that the impact on proliferation or survival of neurons is more common or more severe in MCD-associated NMDAR variants. Alternatively, it has been noted that MCD-associated NMDAR variants tend to have GOF effects.[13] This is consistent with animal models of NMDAR-agonist induced polymicrogyria.[34–36]

In conclusion, the MCD patients with *GRIN1* and *GRIN2B* variants reported to date have overlapping phenotypic features, consisting of early presentation of global developmental delay, epilepsy and microcephaly. Brain imaging mostly shows severe dysgyria, histologically in line with polymicrogyria in two cases, and often with associated brain malformations including dysmorphic basal ganglia and hippocampi. These findings extend our understanding of the “NMDARopathy” spectrum. Our neuropathological findings for the first time provide evidence that *GRIN1* is implicated in the generation, migration and cortical positioning of neurons and interneurons in humans, ultimately leading to MCD.

Acknowledgments

The authors would like to thank the patients, families and scientists who contributed to this work, and Rebecca Bui and Dan Teuscher for technical assistance.

SB, AL, KS, GM, UH, AJ, AEF and NBB are members of the COST Action CA16118 Neuro-MIG.

Competing Interests:

No conflict of interest to declare.

Funding:

The DDD study presents independent research commissioned by the Health Innovation Challenge Fund [grant number HICF-1009-003]. This study makes use of DECIPHER (<http://decipher.sanger.ac.uk>), which is funded by Wellcome. See Nature PMID: 25533962 or www.ddduk.org/access.html for full acknowledgement.

AJ was funded by an FWO Senior Clinical Investigator Fellowship. SB received funding from the Scientific Fund Willy Gepts. DB is supported by NIHR Research Professorship RP-2016-07-011. SFT received funding from the NIH-NINDS (NS111619). HY is supported by the Eunice Kennedy Shriver National Institute of Child Health & Human Development of the National Institutes of Health (R01HD082373) and the National Institute of Mental Health (MH127404). SJM is supported by a grant from the National Institute on Aging (R21AG072142). The content is solely the responsibility of the authors and does not necessarily represent the official views of the National Institutes of Health.

Ethics declaration

Informed consent was obtained from the legal guardians of the patients described in this study. The study was approved by the ethical committee of the UZ Brussel (B.U.N.143201214360). The DDD study was approved by the Cambridge South Research Ethics Committee (10/H0305/83).

REFERENCES

- 1 Cull-Candy S, Brickley S, Farrant M. NMDA receptor subunits: diversity, development and disease. *Curr Opin Neurobiol* 2001;**11**:327–35.
- 2 Traynelis SF, Wollmuth LP, McBain CJ, Menniti FS, Vance KM, Ogden KK, Hansen KB, Yuan H, Myers SJ, Dingledine R. Glutamate Receptor Ion Channels: Structure, Regulation, and Function. *Pharmacol Rev* 2010;**62**:405–96.
- 3 Sobolevsky AI, Beck C, Wollmuth LP. Molecular rearrangements of the extracellular vestibule in NMDAR channels during gating. *Neuron* 2002;**33**:75–85.
- 4 McKay S, Ryan TJ, McQueen J, Indersmitten T, Marwick KFM, Hasel P, Kopanitsa MV, Baxter PS, Martel M-A, Kind PC, Wyllie DJA, O’Dell TJ, Grant SGN, Hardingham GE, Komiyama NH. The Developmental Shift of NMDA Receptor Composition Proceeds Independently of GluN2 Subunit-Specific GluN2 C-Terminal Sequences. *Cell Rep* 2018;**25**:841-851.e4.
- 5 Endelev S, Rosenberger G, Geider K, Popp B, Tamer C, Stefanova I, Milh M, Kortüm F, Fritsch A, Pientka FK, Hellenbroich Y, Kalscheuer VM, Kohlhase J, Moog U, Rappold G, Rauch A, Ropers H-H, von Spiczak S, Tönnies H, Villeneuve N, Villard L, Zabel B, Zenker M, Laube B, Reis A, Wieczorek D, Van Maldergem L, Kutsche K. Mutations in GRIN2A and GRIN2B encoding regulatory subunits of NMDA receptors cause variable neurodevelopmental phenotypes. *Nat Genet* 2010;**42**:1021–6.
- 6 Hamdan FF, Gauthier J, Araki Y, Lin D-T, Yoshizawa Y, Higashi K, Park A-R, Spiegelman D, Dobrzyniecka S, Piton A, Tomitori H, Daoud H, Massicotte C, Henrion E, Diallo O, S2D Group, Shekarabi M, Marineau C, Shevell M, Maranda B, Mitchell G, Nadeau A, D’Anjou G, Vanasse M, Srour M, Lafrenière RG, Drapeau P, Lacaille JC, Kim E, Lee J-R, Igarashi K, Haganir RL, Rouleau GA, Michaud JL. Excess of de novo deleterious mutations in genes associated with glutamatergic systems in nonsyndromic intellectual disability. *Am J Hum Genet* 2011;**88**:306–16.
- 7 Lemke JR, Hendrickx R, Geider K, Laube B, Schwake M, Harvey RJ, James VM, Pepler A, Steiner I, Hörtnagel K, Neidhardt J, Ruf S, Wolff M, Bartholdi D, Caraballo R, Platzer K, Suls A, De Jonghe P, Biskup S, Weckhuysen S. GRIN2B mutations in West syndrome and intellectual disability with focal epilepsy. *Ann Neurol* 2014;**75**:147–54.
- 8 Ohba C, Shiina M, Tohyama J, Haginoya K, Lerman-Sagie T, Okamoto N, Blumkin L, Lev D, Mukaida S, Nozaki F, Uematsu M, Onuma A, Kodera H, Nakashima M, Tsurusaki Y, Miyake N, Tanaka F, Kato M, Ogata K, Saitsu H, Matsumoto N. GRIN1 mutations cause encephalopathy with infantile-onset epilepsy, and hyperkinetic and stereotyped movement disorders. *Epilepsia* 2015;**56**:841–8.
- 9 Lemke JR, Geider K, Helbig KL, Heyne HO, Schütz H, Hentschel J, Courage C, Depienne C, Nava C, Heron D, Møller RS, Hjalgrim H, Lal D, Neubauer BA, Nürnberg P, Thiele H, Kurlmann G, Arnold GL, Bhambhani V, Bartholdi D, Pedurupillay CRJ, Miscio D, Frengen E, Strømme P, Dlugos DJ, Doherty ES, Bijlsma EK, Ruivenkamp CA, Hoffer MJV, Goldstein A, Rajan DS, Narayanan V, Ramsey K, Belnap N, Schrauwen I, Richholt R, Koeleman BPC, Sá J, Mendonça C, de Kovel CGF, Weckhuysen S, Hardies K, De Jonghe P, De Meirleir L, Milh M, Badens C, Lebrun M, Busa T, Francannet C, Piton A, Riesch E, Biskup S, Vogt H, Dorn T, Helbig I, Michaud JL, Laube B, Syrbe S.

- Delineating the GRIN1 phenotypic spectrum: A distinct genetic NMDA receptor encephalopathy. *Neurology* 2016;**86**:2171–8.
- 10 XiangWei W, Jiang Y, Yuan H. De Novo Mutations and Rare Variants Occurring in NMDA Receptors. *Curr Opin Physiol* 2018;**2**:27–35.
 - 11 Rossi M, Chatron N, Labalme A, Ville D, Carneiro M, Edery P, des Portes V, Lemke JR, Sanlaville D, Lesca G. Novel homozygous missense variant of GRIN1 in two sibs with intellectual disability and autistic features without epilepsy. *Eur J Hum Genet* 2017;**25**:376–80.
 - 12 Blakes AJM, English J, Banka S, Basu H. A homozygous GRIN1 null variant causes a more severe phenotype of early infantile epileptic encephalopathy. *Am J Med Genet A* Published Online First: 6 October 2021. doi:10.1002/ajmg.a.62528
 - 13 Fry AE, Fawcett KA, Zelnik N, Yuan H, Thompson BAN, Shemer-Meiri L, Cushion TD, Mugalaasi H, Sims D, Stoodley N, Chung S-K, Rees MI, Patel CV, Brueton LA, Layet V, Giuliano F, Kerr MP, Banne E, Meiner V, Lerman-Sagie T, Helbig KL, Kofman LH, Knight KM, Chen W, Kannan V, Hu C, Kusumoto H, Zhang J, Swanger SA, Shaulsky GH, Mirzaa GM, Muir AM, Mefford HC, Dobyns WB, Mackenzie AB, Mullins JGL, Lemke JR, Bahi-Buisson N, Traynelis SF, Iago HF, Pilz DT. De novo mutations in GRIN1 cause extensive bilateral polymicrogyria. *Brain* 2018;**141**:698–712.
 - 14 Nishimura N, Kumaki T, Murakami H, Enomoto Y, Katsumata K, Toyoshima K, Kurosawa K. Arthrogryposis multiplex congenita with polymicrogyria and infantile encephalopathy caused by a novel GRIN1 variant. *Hum Genome Var* 2020;**7**:29.
 - 15 Platzer K, Yuan H, Schütz H, Winschel A, Chen W, Hu C, Kusumoto H, Heyne HO, Helbig KL, Tang S, Willing MC, Tinkle BT, Adams DJ, Depienne C, Keren B, Mignot C, Frengen E, Strømme P, Biskup S, Döcker D, Strom TM, Mefford HC, Myers CT, Muir AM, LaCroix A, Sadleir L, Scheffer IE, Brilstra E, van Haelst MM, van der Smagt JJ, Bok LA, Møller RS, Jensen UB, Millichap JJ, Berg AT, Goldberg EM, De Bie I, Fox S, Major P, Jones JR, Zackai EH, Abou Jamra R, Rolfs A, Leventer RJ, Lawson JA, Roscioli T, Jansen FE, Ranza E, Korff CM, Lehesjoki A-E, Courage C, Linnankivi T, Smith DR, Stanley C, Mintz M, McKnight D, Decker A, Tan W-H, Tarnopolsky MA, Brady LI, Wolff M, Dondit L, Pedro HF, Parisotto SE, Jones KL, Patel AD, Franz DN, Vanzo R, Marco E, Ranells JD, Di Donato N, Dobyns WB, Laube B, Traynelis SF, Lemke JR. GRIN2B encephalopathy: novel findings on phenotype, variant clustering, functional consequences and treatment aspects. *J Med Genet* 2017;**54**:460–70.
 - 16 Platzer K, Lemke JR. GRIN2B-Related Neurodevelopmental Disorder. In: Adam MP, Ardinger HH, Pagon RA, Wallace SE, Bean LJ, Mirzaa G, Amemiya A, eds. *GeneReviews*®. Seattle (WA): : University of Washington, Seattle 1993. <http://www.ncbi.nlm.nih.gov/books/NBK501979/> (accessed 20 Mar2021).
 - 17 Platzer K, Lemke JR. GRIN1-Related Neurodevelopmental Disorder. In: Adam MP, Ardinger HH, Pagon RA, Wallace SE, Bean LJ, Mirzaa G, Amemiya A, eds. *GeneReviews*®. Seattle (WA): : University of Washington, Seattle 1993. <http://www.ncbi.nlm.nih.gov/books/NBK542807/> (accessed 20 Mar2021).
 - 18 Severino M, Geraldo AF, Utz N, Tortora D, Pogledic I, Klonowski W, Triulzi F, Arrigoni F, Mankad K, Leventer RJ, Mancini GMS, Barkovich JA, Lequin MH, Rossi A.

Definitions and classification of malformations of cortical development: practical guidelines. *Brain* 2020;**143**:2874–94.

- 19 Deciphering Developmental Disorders Study. Large-scale discovery of novel genetic causes of developmental disorders. *Nature* 2015;**519**:223–8.
- 20 Ellard S, Baple EL, Berry I, Forrester N, Turnbull C, Owens M, Eccles DM, Abbs S, Scott R, Deans ZC, Lester T, Campbell J, Newman WG, McMullan DJ. ACGS 2019 Best Practice Guidelines for Variant Classification 2019. 2019. <https://www.leedsth.nhs.uk/assets/Genetics-Laboratory/86fa75f316/ACGS-variant-classification-guidelines-2019.pdf>
- 21 Richards S, Aziz N, Bale S, Bick D, Das S, Gastier-Foster J, Grody WW, Hegde M, Lyon E, Spector E, Voelkerding K, Rehm HL, ACMG Laboratory Quality Assurance Committee. Standards and guidelines for the interpretation of sequence variants: a joint consensus recommendation of the American College of Medical Genetics and Genomics and the Association for Molecular Pathology. *Genet Med* 2015;**17**:405–24.
- 22 Guihard-Costa A-M, Ménez F, Delezoide A-L. Organ weights in human fetuses after formalin fixation: standards by gestational age and body weight. *Pediatr Dev Pathol* 2002;**5**:559–78.
- 23 Moriyoshi K, Masu M, Ishii T, Shigemoto R, Mizuno N, Nakanishi S. Molecular cloning and characterization of the rat NMDA receptor. *Nature* 1991;**354**:31–7.
- 24 Oegema R, Cushion TD, Phelps IG, Chung S-K, Dempsey JC, Collins S, Mullins JGL, Dudding T, Gill H, Green AJ, Dobyns WB, Ishak GE, Rees MI, Doherty D. Recognizable cerebellar dysplasia associated with mutations in multiple tubulin genes. *Hum Mol Genet* 2015;**24**:5313–25.
- 25 Hebebrand M, Hüffmeier U, Trollmann R, Hehr U, Uebe S, Ekici AB, Kraus C, Krumbiegel M, Reis A, Thiel CT, Popp B. The mutational and phenotypic spectrum of TUBA1A-associated tubulinopathy. *Orphanet J Rare Dis* 2019;**14**:38.
- 26 Jiang H, Jiang W, Zou J, Wang B, Yu M, Pan Y, Lin Y, Mao Y, Wang Y. The GluN2B subunit of N-methyl-D-aspartate receptor regulates the radial migration of cortical neurons in vivo. *Brain Res* 2015;**1610**:20–32.
- 27 Soria JM, Valdeolmillos M. Receptor-activated calcium signals in tangentially migrating cortical cells. *Cereb Cortex* 2002;**12**:831–9.
- 28 Swanger SA, Chen W, Wells G, Burger PB, Tankovic A, Bhattacharya S, Strong KL, Hu C, Kusumoto H, Zhang J, Adams DR, Millichap JJ, Petrovski S, Traynelis SF, Yuan H. Mechanistic Insight into NMDA Receptor Dysregulation by Rare Variants in the GluN2A and GluN2B Agonist Binding Domains. *Am J Hum Genet* 2016;**99**:1261–80.
- 29 Mullier B, Wolff C, Sands ZA, Ghisdal P, Muglia P, Kaminski RM, André VM. GRIN2B gain of function mutations are sensitive to radiprodil, a negative allosteric modulator of GluN2B-containing NMDA receptors. *Neuropharmacology* 2017;**123**:322–31.
- 30 Takahashi H, Shin Y, Cho S-J, Zago WM, Nakamura T, Gu Z, Ma Y, Furukawa H, Liddington R, Zhang D, Tong G, Chen H-SV, Lipton SA. Hypoxia enhances S-

- nitrosylation-mediated NMDA receptor inhibition via a thiol oxygen sensor motif. *Neuron* 2007;**53**:53–64.
- 31 Sullivan JM, Traynelis SF, Chen HS, Escobar W, Heinemann SF, Lipton SA. Identification of two cysteine residues that are required for redox modulation of the NMDA subtype of glutamate receptor. *Neuron* 1994;**13**:929–36.
 - 32 Brimecombe JC, Boeckman FA, Aizenman E. Functional consequences of NR2 subunit composition in single recombinant N-methyl-D-aspartate receptors. *Proc Natl Acad Sci U S A* 1997;**94**:11019–24.
 - 33 Bell S, Maussion G, Jefri M, Peng H, Theroux J-F, Silveira H, Soubannier V, Wu H, Hu P, Galat E, Torres-Platas SG, Boudreau-Pinsonneault C, O’Leary LA, Galat V, Turecki G, Durcan TM, Fon EA, Mechawar N, Ernst C. Disruption of GRIN2B Impairs Differentiation in Human Neurons. *Stem Cell Reports* 2018;**11**:183–96.
 - 34 Marret S, Mukendi R, Gadisseux JF, Gressens P, Evrard P. Effect of ibotenate on brain development: an excitotoxic mouse model of microgyria and posthypoxic-like lesions. *J Neuropathol Exp Neurol* 1995;**54**:358–70.
 - 35 Takano T, Sawai C, Takeuchi Y. Radial and tangential neuronal migration disorder in ibotenate-induced cortical lesions in hamsters: immunohistochemical study of reelin, vimentin, and calretinin. *J Child Neurol* 2004;**19**:107–15.
 - 36 Takano T, Matsui K. Increased expression of GAP43 in interneurons in a rat model of experimental polymicrogyria. *J Child Neurol* 2015;**30**:716–28.

FIGURES

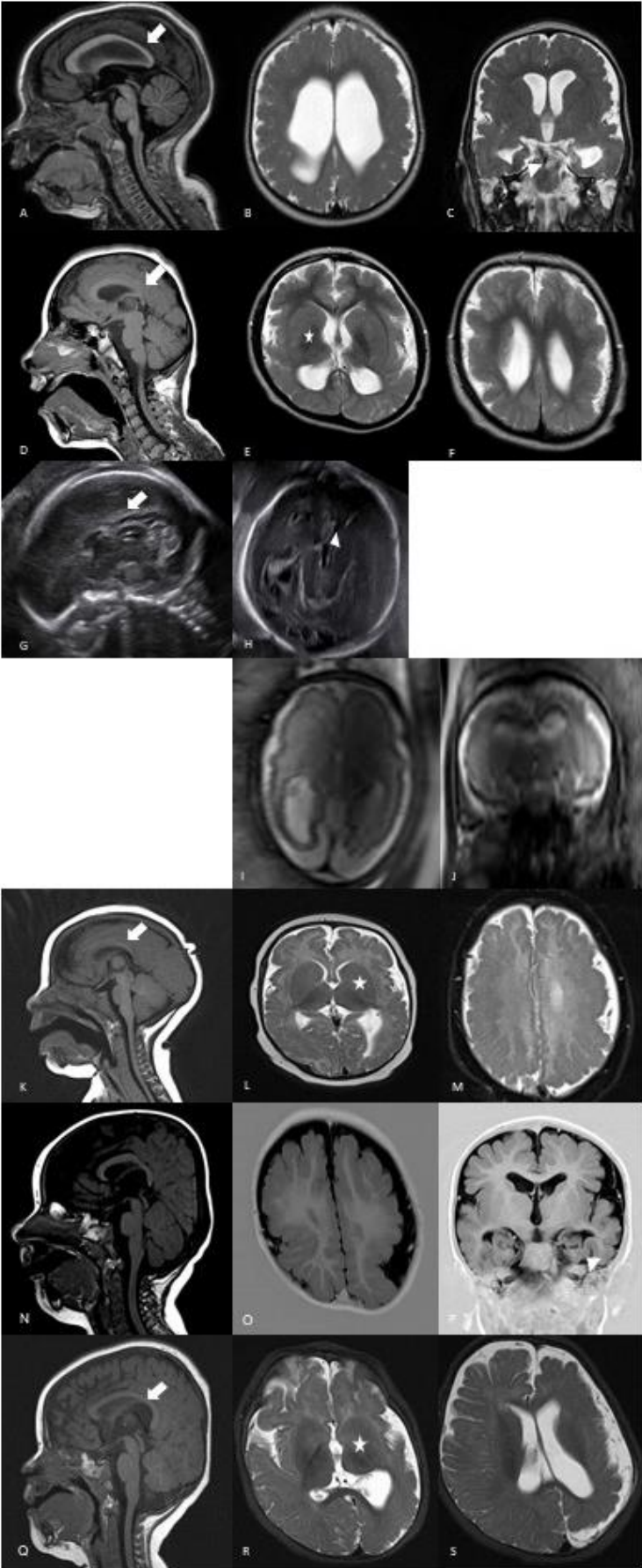


Figure 1: Brain imaging findings of individuals with heterozygous pathogenic variants in *GRIN1* and *GRIN2B* . Individual 1 has diffuse dysgyria, hypoplastic corpus callosum (arrow) and dysmorphic hippocampi (arrowhead) (A-C). Individual 2 has bilateral dysgyria, hypoplastic corpus callosum (arrow) and dysmorphic basal ganglia (asterisk) (D-F). Prenatal ultrasound in individual 3 at 25 gestational weeks shows absent corpus callosum (arrow) and dilated third ventricle (arrowhead) (G-H). Individual 4 has diffuse dysgyria and enlarged lateral ventricles on prenatal MRI at 29 gestational weeks (I-J). Individual 5 presents with bilateral dysgyria, enlarged basal ganglia (asterisk) and hypoplastic corpus callosum (arrow) (K-M). Individual 6 has bilateral symmetric dysgyria and dysmorphic hippocampi (arrowhead) (N-P). Individual 7 has asymmetric dysgyria of the left hemisphere, dysmorphic basal ganglia (asterisk) and corpus callosum (arrow) (Q-S).

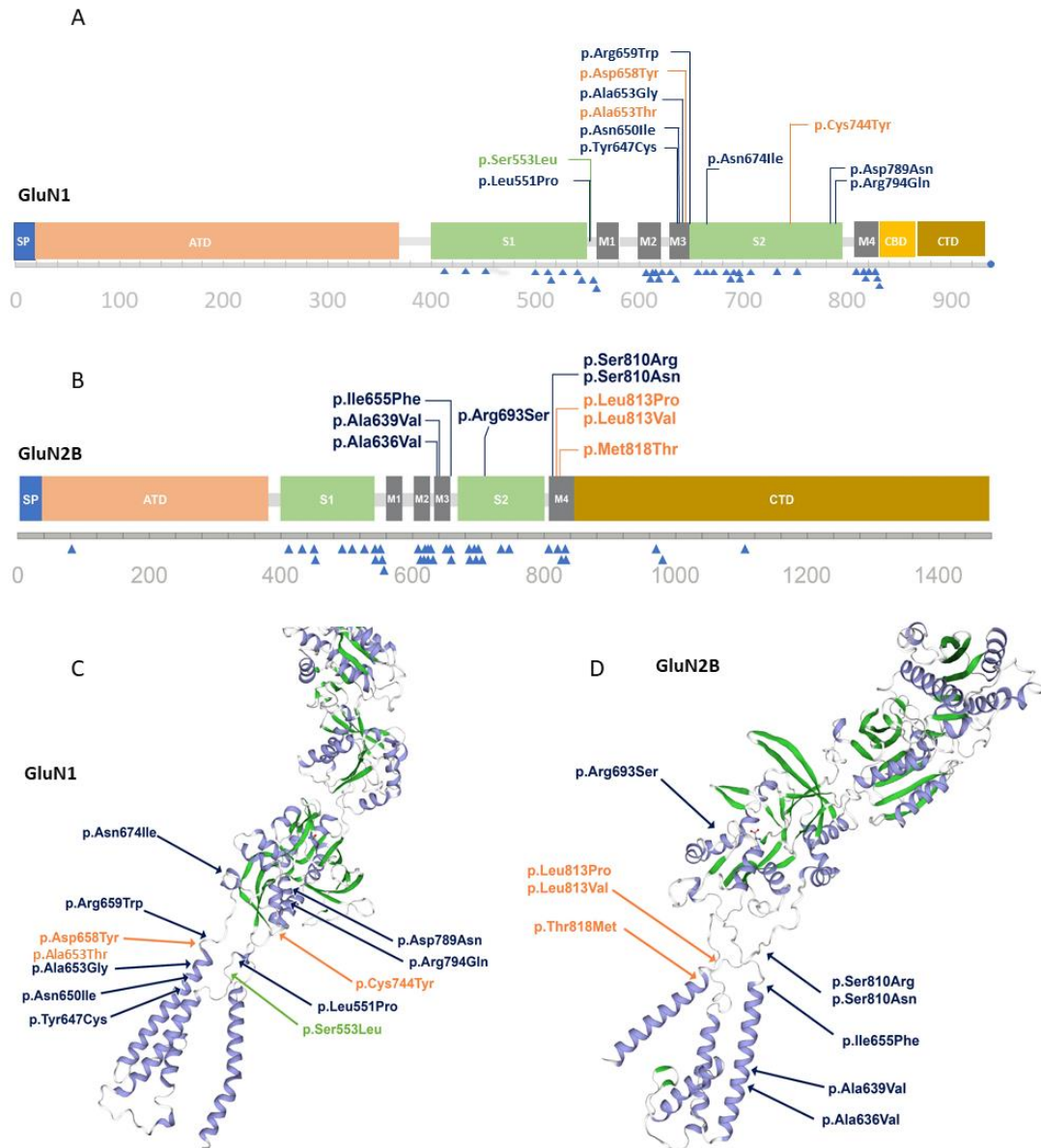


Figure 2: Distribution of variants in linear model and 3D protein structure for *GRIN1* (A, C) and *GRIN2B* (B, D). In the linear model, clustering of MCD-associated variants (top) and non-MCD associated variants (bottom, blue triangles) is highlighted. Functional domains are highlighted in the 3D model: blue – helices, green – sheets. Reported variants from this cohort are written in orange, variants reported in the literature are blue, the recurring variant in the literature and our cohort is green. The 3D structure is based on Swiss Models NMDZ1_HUMAN Glutamate receptor ionotropic, NMDA1 Q05586 and NMDE2_HUMAN Q13224 Glutamate receptor ionotropic, NMDA 2B.

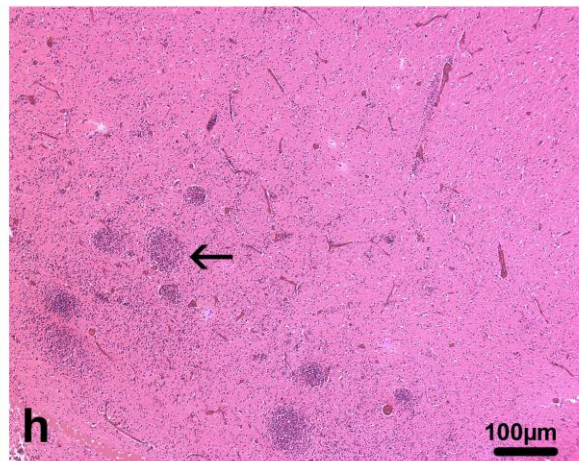
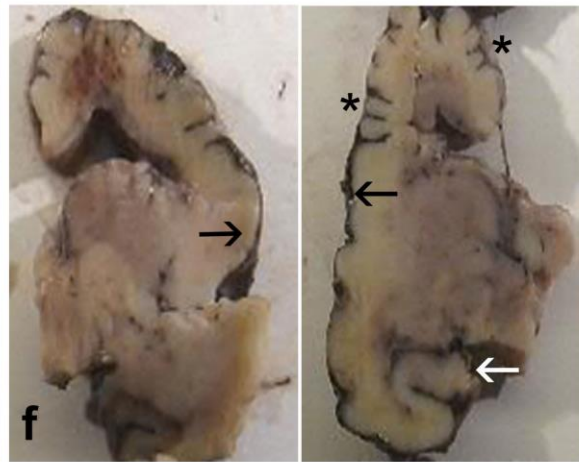
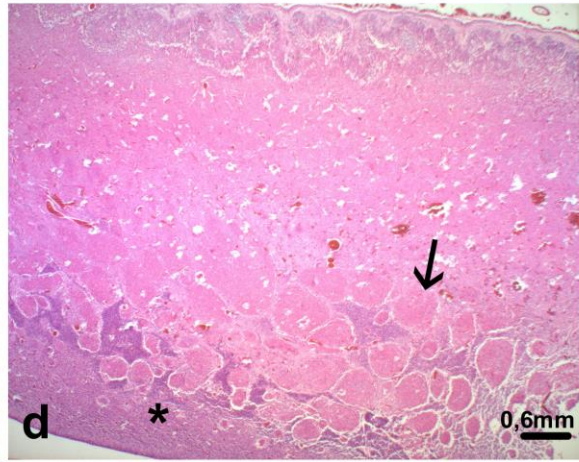


Figure 3: Distinctive brain morphological characteristics from individuals 3 and 4

Individual 3: A) External view of the left side of the brain, where primary fissures are lacking, with almost indiscernible Sylvian fissure (arrow) and marked temporal lobe hypoplasia (blue asterisk), B) compared to an age matched control brain, where the Sylvian fissure has a triangular shape (arrow). C) The brain surface is smooth with a relatively thick transient subpial granular cell layer which should have been disappeared from 22 WG (arrow) and diffuse micropolygyria forming multiple protrusions into the molecular layer [OM x 20]. D) The cerebral mantle is particularly thin (half of the thickness of a normal cortical plate) and the deep intermediate zone contains numerous heterotopic nodules of various sizes (arrow) above the germinative zone of the dorsal telencephalon (asterisk) [OM x 20].

Individual 4: E) Median supratentorial sagittal section revealing posterior hypoplasia of the corpus callosum (white arrow), F) and on coronal sections, supernumerary gyri (asterisks), areas of smoothed cortex covering polymicrogyria (black arrows) and malrotated hippocampus (white arrow). G) Characteristic histological features of unlayered polymicrogyria [H&E, OM x 50], H) associated with confetti-like nodular heterotopias, measuring about 1.50 μ , distributed throughout the intermediate zone (arrow) [H&E, OM x 50].

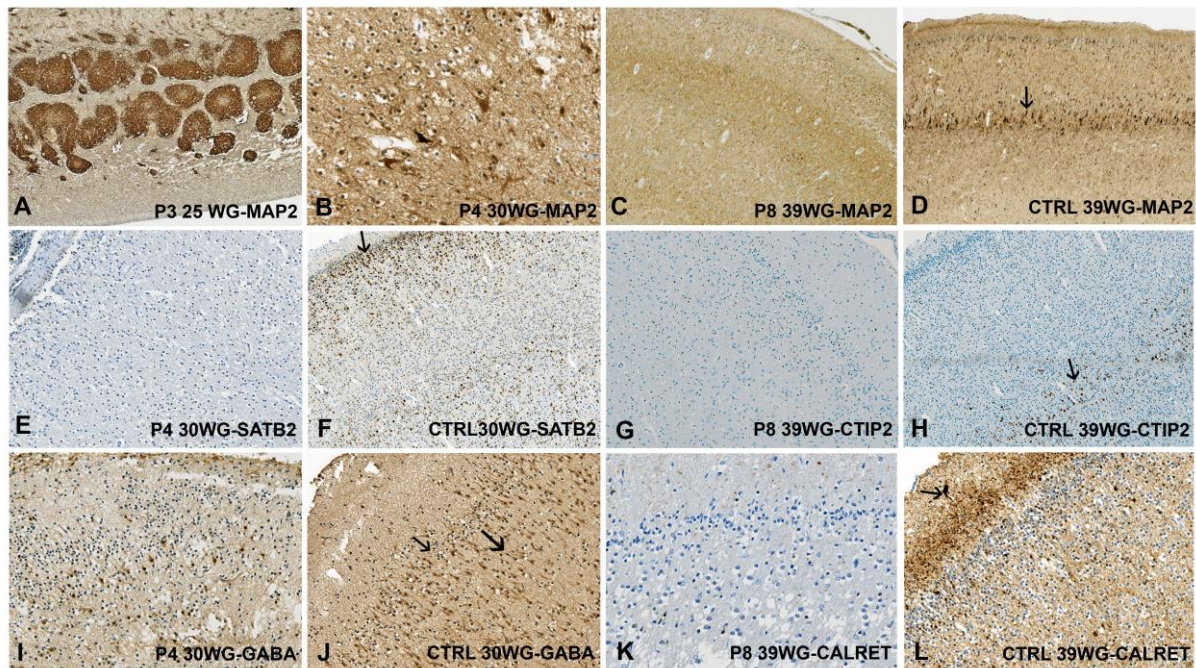


Figure 4: Immunohistochemical findings in individuals 3, 4 and 8

A) Strong MAP2 immunoreactivity in the periventricular heterotopic nodules in individual 3.

B) Scattered dysmorphic MAP2-positive pyramidal neurons in the cortical plate (individual 4).

C) Decreased density in MAP2-positive haphazardly dispersed pyramidal neurons in the cortical plate (individual 8), D) compared to the control cortical plate aged 39 WG in which neurons of layers II, III and V with predominance in layer V (arrow).

E) Almost no SATB2-positive neurons in the cortex of individual 4, F) contrary to the control brain aged 30 WG where SATB2 positive neurons are observed mainly in layer II (arrow) and to a lesser extent in Layers III and IV.

G) No CTIP2 immunoreactive neurons (individual 8), H) whereas in the control cortical plate, immunoreactive neurons are observed mainly in layer V (arrow).

I) Few GABAergic interneurons dispersed in the micropolygyric cortex (individual 4), J) by comparison with the control brain where GABA antibody immunolabels interneurons of layers I, II (thin arrow) and III (thick arrow), K) and with scarce calretininergic interneurons

in layer III (individual 8), L) conversely to the control, where calretinin antibody immunolabels the tangential superficial network and Cajal Retzius cells (arrow) in layer I, interneurons in layers II and III.

Dark brown staining: specific, light brown: background staining; 25 WG: individual 3; 30 WG: individual 4; 39 WG: individual 8.

Abbreviations: BG – basal ganglia, CC – corpus callosum, H&E – haematoxylin-eosin staining, OM – original magnification.

Supplementary data

1. Literature review of clinical features of *GRIN1* and *GRIN2B*- associated MCD
 - a. Supplementary table 1: Clinical and imaging features of patients with variants in *GRIN1*
 - b. Supplementary table 2: Clinical and imaging features of patients with variants in *GRIN2B*
 - c. Supplementary table 3: Abnormal brain MRI findings in NMDAR MCD patients.
2. Molecular data
 - a. Supplementary table 4: ACMG-AMP criteria used to classify the NMDAR variants
 - b. Supplementary table 5: *In silico* predictions for the NMDAR missense variants
3. Electrophysiological studies
 - a. Methods
 - b. Results
4. Neuropathology
 - a. Methods
 - b. Supplementary table 6: Antibodies used for the study
 - c. Supplementary table 7: Comparative semi-quantitative analysis of immunolabelling in the germinative and intermediate zones as well as in the different layers of the frontal cortex of affected and control patients
 - d. Supplementary figure 1: Main brain macroscopic and histological findings of individual 8

1. Literature review of clinical features of *GRIN1* and *GRIN2B*- associated MCD

a. Supplementary Table 1 – Clinical and imaging features of patients with variants in *GRIN1*

	Fry et al. - P1	Fry et al. - P2	Fry et al. - P3	Fry et al. - P4	Fry et al. - P5	Fry et al. - P6	Fry et al. - P7	Fry et al. - P8	Fry et al. - P9	Fry et al. - P10	Fry et al. - P11	Nishimura et al., 2020	P1 (This paper)	P2 (This paper)	P3 (This paper)	P4 (This paper)
Pathogenic variant	c.2021A>T, p.(Asn674Ile)	c.2381G>A, p.(Arg794Gln)	c.1975C>T, p.(Arg659Trp)	c.1940A>G, p.(Tyr647Cys)	c.2365G>A, p.(Asp789Asn)	c.1652T>C, p.(Leu551Pro)	c.1958C>G, p.(Ala653Gly)	c.1949A>T, p.(Asn650Ile)	c.1975C>T, p.(Arg659Trp)	c.2365G>A, p.(Asp789Asn)	c.1658C>T, p.(Ser553Leu)	c.1949A>C, p.(Asn650Thr)	c.1658C>T, p.(Ser553Leu)	c.1972G>T, p.(Asp658Tyr)	c.1957G>A, p.(Ala653Thr)	c.2231G>A, p.(Cys744Tyr)
Microcephaly (at last control)	- 3.6SD	- 5.2 SD	- 7.1 SD	- 1.5 SD	- 6.5 SD	n/a	- 1.6 SD	- 5.7 SD	n/a	- 6.7 SD	- 7.1 SD	- 2.7 SD	- 5.2 SD	- 2 SD	reduced brain weight, -2 SD	n/a (reduced brain weight)
Development	Severe delay	Severe delay	Severe delay	Severe delay	Severe delay	Severe delay	Severe delay	Severe delay	Severe delay	Severe delay	Severe delay	n/a	Severe delay	Severe delay	n/a	n/a
Neurology	Spastic tetraplegia, axial hypotonia	Spastic tetraplegia, axial hypotonia	Spastic tetraplegia, axial hypotonia	Pseudobulbar palsy, hypotonia	Spastic tetraplegia, axial hypotonia	Spastic tetraplegia, axial hypotonia	n/a	Spastic tetraplegia, axial hypotonia	Mild scoliosis	Spastic tetraplegia, axial hypotonia	Spastic tetraplegia, axial hypotonia	n/a	Hypertonia	Hypo- and hypertonia	n/a	n/a
Onset of seizures	6 W	9 M	2 M	3 M	1 W	1 Y	n/a	1 M	5 W	1 M	2 W	Neonatal	Possibly prenatally	4 M	n/a	n/a
Type of seizures	Myoclonic	Generalized tonic-clonic	Spasms	Tonic	Grimacing	Spasms	n/a	Tonic	Tonic	Gaze deviation	Tonic	Focal	n/a	Absences, drops, tonic extensions	n/a	n/a
Cortical visual impairment	Yes	Yes	Yes	Yes	Yes	Yes	n/a	Yes	n/a	Yes	Yes	n/a	Poor vision	Yes	n/a	n/a
Movement disorders	n/a	n/a	n/a	Yes	n/a	Yes	n/a	Gaze deviations	n/a	Gaze deviations	n/a	Yes	No	No	n/a	n/a
Contractures	n/a	n/a	n/a	n/a	n/a	n/a	n/a	n/a	n/a	n/a	n/a	Yes	No	Scoliosis	n/a	No
Cortex	Dysgyria	Dysgyria	Dysgyria	Dysgyria	Dysgyria	Dysgyria	Dysgyria	Dysgyria	Dysgyria	Dysgyria	Dysgyria	Dysgyria	Dysgyria	Dysgyria	Dysgyria	Dysgyria
Bilateral	Yes	Yes	Yes	Yes	Yes	Yes	Yes	Yes	Yes	Yes	Yes	Yes	Yes	Yes	Yes	Yes
Diffuse			Yes				n/a			Yes	Yes				n/a	n/a
A>P gradient	Yes	Yes		Yes	Yes	Yes	n/a	Yes	Yes			Yes	Yes	Yes	n/a	n/a
Perisylvian	Affected	Affected	Affected	Affected	Affected	Affected	Affected	Affected	Affected	Affected	Affected	Affected	Affected	Affected	Affected	Affected
Asymmetrical	No	No	No	No	No	No	L>R	No	No	No	No	No	No	No	No	No
White matter	Normal	Reduced	n/a	Reduced	Reduced	n/a	n/a	Reduced	Reduced	Reduced	Reduced	Normal	Reduced	Reduced	n/a	n/a
Ventricles	Normal	Mildly enlarged	n/a	Mildly enlarged	Mildly enlarged	Normal	Enlarged	Enlarged	Moderately enlarged	Enlarged	Enlarged	Mildly enlarged	Enlarged	Enlarged	Enlarged	Enlarged
Periventricular region	Normal	Reduced white matter	n/a	n/a	n/a	n/a	n/a	Reduced white matter	n/a	n/a	n/a	Normal	Reduced white matter			
Corpus callosum	Normal	Normal	Thin	Normal	Normal	Normal	Hypoplastic	Thin	Normal	Normal	Thin	n/a	Hypoplastic	Normal	ACC	Hypoplastic
Basal ganglia	Normal	Normal	Normal	Normal	Normal	Normal	n/a	Mildly dysmorphic	Mildly dysmorphic	Mildly dysmorphic	Mildly dysmorphic	Mildly dysmorphic	Normal	Dysmorphic	Normal	Dysplastic
Brain stem	Normal	Normal	Normal	n/a	n/a	n/a	Normal	Normal	Normal	Normal	Normal	n/a	Abnormal myelination	Normal	Normal	Normal
Cerebellum	Normal	Normal	Normal	n/a	n/a	n/a	Mildly enlarged	Normal	Normal	Normal	Normal	Normal	Normal	Normal	Enlarged	Hypoplastic
Hippocampus	Normal	Normal	n/a	Normal	Abnormal	Normal	Normal	Abnormal	Normal	Normal	Thin leaves	Normal	Dysmorphic	Normal	Normal	Dysmorphic
Other features																Operculum of sylvian fissure, enlarged subarachnoid spaces

b. Supplementary Table 2 – Clinical and imaging features of patients with variants in *GRIN2B*

	Platzter et al. 2017	Platzter et al. 2017	Platzter et al. 2017	Platzter et al. 2017	Platzter et al. 2017	Platzter et al. 2017	P5 (This paper)	P6 (This paper)	P7 (This paper)
Pathogenic variant	c.1907C>T, p.(Ala636Val)	c.1916C>T, p.(Ala639Val)	c.1963A>T, p.(Ile655Phe)	c.2079A>T, p.(Arg693Ser)	c.2430C>A, p.(Ser810Arg)	c.2429G>A, p.(Ser810Asn)	c.2437C>G, p.(Leu813Val)	c.2438T>C, p.(Leu813Pro)	c. 2453T>C, p.(Met818Thr)
Microcephaly	Yes	n/a	Yes	n/a	Yes	n/a	- 3.2 SD	- 2.2 SD	- 3.9 SD
Development	Severe delay	Severe delay	Severe delay	Severe delay	Severe delay	Severe delay	Severe delay	Severe delay	Severe delay
Neurology							Truncal hypotonia, limb hypertonia	Truncal hypotonia, limb hypertonia, pseudobulbar palsy	Hypertonia
Onset of seizures							4 M	2 Y 3 M	10 W
Type of seizures	Focal seizures, epileptic spasms	Focal and generalized seizures	Generalized seizures, epileptic spasms	Generalized and focal seizures, epileptic spasms	Focal seizures	Generalized seizures, epileptic spasms	Epileptic spasms	GTC with fever	Rapid and rolling eye movements
Cortical visual impairment	Yes	Yes	Yes				No but strabism	Yes	n/a
Movement disorders							No		
Contractures							No		
Cortex	Dysgyria	Dysgyria	Dysgyria	Dysgyria	Dysgyria	Dysgyria	Dysgyria	Dysgyria	Dysgyria
Bilateral	Yes	Yes	Yes	Yes	Yes	Yes	Yes	Yes	Yes
Diffuse	Yes	Yes	Yes	Yes	Yes	Yes	Yes		
A>P gradient								Yes	Yes
Perisylvian	Affected	Affected	Affected	Affected	Affected	Affected	Affected	Affected	Affected
Asymmetrical	No	No	No	No	No	No	No	No	Yes, left > right
White matter	Affected	Affected	Affected	Affected	Affected	Affected	Occipitally reduced	Reduced	Reduced
Ventricles	n/a	Severely enlarged	Mildly enlarged	Enlarged	Severely enlarged	Severely enlarged	Colpocephaly	Enlarged	Enlarged (left)
Periventricular region	n/a	Normal	Normal	Normal	Normal	Normal	Normal	Normal	Normal
Corpus callosum	Normal	Hypoplastic	Normal	Normal	Hypoplastic	Hypoplastic	Hypoplastic	Normal	Dysmorphic
Basal ganglia	Dysmorphic	Dysmorphic	Dysmorphic	Dysmorphic	Dysmorphic	Dysmorphic	Enlarged	Normal	Dysmorphic
Brain stem	Normal	Normal	Normal	Normal	Normal	Normal	Normal	Normal	Normal
Cerebellum	Normal	Normal	Normal	Normal	Normal	Normal	Normal	Normal	Normal
Hippocampus	Dysplastic	Dysplastic	Dysplastic	Normal	Dysplastic	Normal	Normal	Dysmorphic	Normal

B.**Supplementary table 3. Abnormal brain MRI findings in NMDAR MCD patients.**

MRI	This series		Cases reported in the literature	
	GRIN1	GRIN2B	GRIN1	GRIN2B
Dysgyria	4/4	3/3	12/12	6/6
Bilateral	4/4	3/3	12/12	6/6
Diffuse	0/2	2/3	3/11	6/6
A>P Gradient	2/2	2/3	8/11	0/6
Perisylvian fissure	3/3	3/3	12/12	6/6
Asymmetry	0/4	1/3	1/12	0/6
White matter	2/2	3/3	7/9	6/6
Lateral ventricles	4/4	3/3	9/11	5/5
Corpus callosum	3/4	1/3	4/11	3/6
Basal ganglia	2/4	2/3	4/10	6/6
Brainstem	1/4	0/3	0/8	0/6
Cerebellum	2/4	0/3	1/9	0/6
Hippocampus	2/4	1/3	3/11	4/6

Abbreviations: A>P, anterior-to-posterior gradient with anterior regions more affected by dysgyria

2. Molecular data

a. Supplementary Table 4. ACMG-AMP criteria used to classify the NMDAR variants.

Gene	Mutation	ACMG-AMP Criteria	Classification
<i>GRIN1</i>	p.(Tyr474*)	PM2, PVS1, PM3_supporting	Pathogenic
<i>GRIN1</i>	p.(Ser553Leu)	PM2, PP2, PP3, PS2_strong, PM1	Pathogenic
<i>GRIN1</i>	p.(Ala653Thr)	PM2, PP2, PP3, PS2_moderate, PM1	Likely pathogenic
<i>GRIN1</i>	p.(Asp658Tyr)	PM2, PP2, PP3, PS2_moderate, PM1	Likely pathogenic
<i>GRIN1</i>	p.(Cys744Tyr)	PM2, PP2, PP3, PS2_moderate, PM1, PS3_moderate	Likely pathogenic
<i>GRIN2B</i>	p(Leu813Val)	PM2, PP2, PP3, PM5, PS2_moderate, PM1	Likely pathogenic
<i>GRIN2B</i>	p.(Leu813Pro)	PM2, PP2, PP3, PM5 PS2_moderate, PM1	Likely pathogenic
<i>GRIN2B</i>	p.(Met818Thr)	PM2, PP2, PP3, PS2_strong, PM1	Pathogenic

b. **Supplementary Table 5. *In silico* predictions for the NMDAR missense variants and the homozygous *GRIN1* variants**

Gene	<i>GRIN1</i>	<i>GRIN1</i>	<i>GRIN1</i>	<i>GRIN1</i>	<i>GRIN2B</i>	<i>GRIN2B</i>	<i>GRIN2B</i>	<i>GRIN1</i>
Mutation (NM_007327.3, NM_000834.3)	c.1658C>T, p.S553L	c.1972G>T, p.D658Y	c.1957G>A, p.A653T	c.2231G>A, p.C744Y	c.2437C>G, p.L813V	c.2438T>C, p.L813P	c.2453T>C, p.M818T	c.1422C>A, p.Y474*
Genomic position (hg19)	chr9:g.140056649C>T	chr9:g.140057150G>T	chr9:140057135G>A	chr9:g.140057680G>A	chr12:g.13720120G>C	chr12:g.13720119A>G	chr12:g.13720104A>G	chr9:140055823C>A
SIFT	0.001 (Damaging)	0 (Damaging)	0.001 (Damaging)	0 (Damaging)	-	-	-	-
Polyphen2 (HDIV)	1 (Probably damaging)	1 (Probably damaging)	0.999 (Probably damaging)	-				
Polyphen2 (HVAR)	1 (Probably damaging)	1 (Probably damaging)	1 (Probably damaging)	1 (Probably damaging)	0.999 (Probably damaging)	1 (Probably damaging)	0.999 (Probably damaging)	-
LRT	0 (Unknown)	0 (Deleterious)	0 (Deleterious)	0 (Deleterious)	0 (Deleterious)	0 (Deleterious)	0 (Deleterious)	0 (Unknown)
MutationTaster	1 (Disease causing)	1 (Disease causing)	1 (Disease causing)	-				
MutationAssessor	3.415 (Medium)	2.645 (Medium)	3.21 (Medium)	3.91 (High)	3.085 (Medium)	3.23 (Medium)	2.395 (Medium)	-
FATHMM	2.01 (Tolerable)	0.55 (Tolerable)	-0.32 (Tolerable)	0.51 (Tolerable)	-	-	-	-
PROVEAN	-5.03 (Damaging)	-6 (Damaging)	-3.35 (Damaging)	-9.82 (Damaging)	-	-	-	-
VEST3	0.899 (Damaging)	0.574 (Damaging)	0.749 (Damaging)	0.99 (Damaging)	0.851 (Damaging)	0.981 (Damaging)	0.935 (Damaging)	-
MetaSVM	-0.447 (Tolerable)	-0.328 (Tolerable)	0.018 (Damaging)	0.227 (Damaging)	0.106 (Damaging)	0.257 (Damaging)	-0.36 (Tolerable)	-
MetaLR	0.202 (Tolerable)	0.34 (Tolerable)	0.486 (Tolerable)	0.473 (Tolerable)	0.503 (Damaging)	0.547 (Damaging)	0.329 (Tolerable)	-
M_CAP	0.425 (Damaging)	0.914 (Damaging)	0.823 (Damaging)	0.48 (Damaging)	0.606 (Damaging)	0.919 (Damaging)	0.551 (Damaging)	-
CADD	32 (Damaging)	26.7 (Damaging)	28.1 (Damaging)	28.4 (Damaging)	25.4 (Damaging)	28.2 (Damaging)	26 (Damaging)	36 (Damaging)

	g)	g)	g)	g)	g)	g)	g)	g)
DANN	0.999 (Damagin g)	0.995 (Damagin g)	0.999 (Damagin g)	0.997 (Damagin g)	0.998 (Damagin g)	0.999 (Damagin g)	0.994 (Damagin g)	0.995 (Damagin g)
FATHMM_ MKL	0.937 (Damagin g)	0.96 (Damagin g)	0.944 (Damagin g)	0.955 (Damagin g)	0.974 (Damagin g)	0.985 (Damagin g)	0.985 (Damagin g)	0.283 (Tolerable)
Eigen	0.578 (Damagin g)	0.604 (Damagin g)	0.623 (Damagin g)	0.874 (Damagin g)	0.638 (Damagin g)	0.868 (Damagin g)	0.807 (Damagin g)	-0.385 (Tolerable)
GenoCanyon	1 (Damagin g)	1 (Damagin g)	1 (Damagin g)	1 (Damagin g)	1 (Damagin g)	1 (Damagin g)	1 (Damagin g)	1 (Damagin g)
fitCons	0.598 (Tolerable)	0.658 (Tolerable)	0.658 (Tolerable)	0.652 (Tolerable)	0.554 (Tolerable)	0.554 (Tolerable)	0.554 (Tolerable)	0.598 (Tolerable)
GERP	3.83 (Conserve d)	3.63 (Conserve d)	3.63 (Conserve d)	4.97 (Conserve d)	4.54 (Conserve d)	5.43 (Conserve d)	5.43 (Conserve d)	-3.09 (Nonconse rved)
phyloP	5.468 (Conserve d)	9.153 (Conserve d)	9.582 (Conserve d)	9.314 (Conserve d)	5.025 (Conserve d)	9.32 (Conserve d)	9.32 (Conserve d)	-1.601 (Nonconse rved)
phastCons	1 (Conserve d)	1 (Conserve d)	1 (Conserve d)	1 (Conserve d)	1 (Conserve d)	1 (Conserve d)	1 (Conserve d)	0.0001 (Nonconse rved)
SiPhy	14.305 (Conserve d)	12.526 (Conserve d)	12.526 (Conserve d)	16.773 (Conserve d)	14.17 (Conserve d)	15.484 (Conserve d)	15.484 (Conserve d)	10.605 (Nonconse rved)
REVEL	0.655 (Damagin g)	0.469 (Damagin g)	0.676 (Damagin g)	0.776 (Damagin g)	0.61 (Damagin g)	0.855 (Damagin g)	0.781 (Damagin g)	-
ReVe	0.888 (Damagin g)	0.721 (Damagin g)	0.869 (Damagin g)	0.98 (Damagin g)	0.893 (Damagin g)	0.988 (Damagin g)	0.96 (Damagin g)	0.416 (Tolerable)
ClinPred	0.9751868 4 (pathogeni c)	0.9988429 5 (pathogeni c)	0.9969938 9 (pathogeni c)	0.9999705 (pathogeni c)	0.9870252 0 (pathogeni c)	0.9954946 9 (pathogeni c)	0.9913973 5 (pathogeni c)	-

Derived from Varcards <http://159.226.67.237/sun/varcards/>

3. Functional evaluation of a human glutamate receptor variant p.Cys744Tyr in *GRIN1* *in vitro*

a. METHODS

cDNA Plasmid Constructs: The p.Cys744Tyr and the p.Ala653Thr *GRIN1* variants were introduced into a GluN1 cDNA (RefSeq NM.007327.3) plasmid construct, and the p.Ala653Thr *GRIN2B* variant into the GluN2B cDNA (RefSeq NM_000834.3) via a Quikchange (Agilent) mutagenesis protocol. All experiments used cDNAs encoding human gene sequences verified with Sanger sequencing (Eurofins). mRNA was synthesized from cDNA using mMESSAGE mMACHINE (Invitrogen).

mRNA Injections: The cRNAs for GluN1-C744Y, GluN1-A653T or GluN1-WT were combined, separately, with human GluN2A-WT cRNA, or GluN1-WT and GluN2B-M818T were combined separately, and injected into stage V and VI oocytes and incubated at 16 C for 2–7 days in Barth's culture medium containing (in mM): 88 NaCl, 2.4 NaHCO₃, 1 KCl, 0.33 Ca(NO₃)₂, 0.41 CaCl₂, 0.82 MgSO₄, and 5 Tris/HCl (pH 7.4). For experiments, oocytes were removed from the incubator and perfused in recording Barth's solution for two-electrode voltage clamp (TEVC) electrophysiological recordings. Conditions for each experiment are below.

L-Glutamate dose response studies: The recording solution for these studies contained (in mM): NaCl (90), KCl (1.0), BaCl₂ (0.5), HEPES (10), and EDTA (0.01), adjusted to pH 7.4 (at 23 degrees C) with NaOH. The oocyte membrane potential was clamped at -40 mV. After a steady baseline was obtained, oocytes were perfused with increasing concentrations of L-glutamate (seven concentrations selected from 0.003, 0.01, 0.03, 0.1, 0.3, 1, 3, 10, 30, and 100 μM) for 0.75 min duration each in the continuous presence of 100 μM glycine. Results at each L-glutamate concentration were normalized to the maximum receptor activation levels (defined as 100%) and the EC₅₀ values obtained by fitting concentration-response data with Equation 1 (below).

Glycine dose response studies: The recording solution for these studies was similar as for the L-glutamate studies. The oocyte membrane potential was clamped at -40 mV. After a steady baseline was obtained, oocytes were perfused with increasing concentrations of glycine (seven concentrations selected from 0.003, 0.01, 0.03, 0.1, 0.3, 1, 3, 10, 30 and 100 μM) for 0.75 min duration each in the continuous presence of 100 μM L-glutamate. Results at each glycine concentration were normalized to the maximum receptor activation levels (defined as 100%) and the EC₅₀ values obtained by fitting concentration-response data with Equation 1 (below).

Mg²⁺ dose inhibition studies: The recording solution for Mg²⁺ studies contained (in mM): NaCl (90), KCl (1.0), BaCl₂ (0.5), and HEPES (10) adjusted to pH 7.4 (at 23 degrees C) with NaOH. The oocyte membrane potential was clamped at -60 mV. After a steady baseline was obtained, oocytes were maximally activated with 100 μM L-glutamate and 100 μM glycine and were then perfused with increasing concentrations of Mg²⁺ (3, 10, 30, 100, 300, and 1000 μM) in the presence of maximal glutamate and glycine. The current responses to glutamate and glycine at each Mg²⁺ concentration were normalized to the maximum receptor activation levels in the absence of Mg²⁺ (defined as 100%) and the IC₅₀ values obtained by fitting concentration-inhibition data with Equation 2 (below).

pH studies: The recording solution for these studies contained (in mM): NaCl (90), KCl (1.0), BaCl₂ (0.5), HEPES (10), and EDTA (0.01), adjusted to either pH 6.8 or pH 7.6 (at 23 degrees C) with HCl or NaOH. The oocyte membrane potential was clamped at -40 mV. After a steady baseline was obtained in pH 7.6 recording buffer the oocytes were maximally activated with 100 μM L-glutamate and 100 μM glycine in pH 7.6 buffer. Following a washout period to reestablish baseline, the oocytes were then maximally activated with 100 μM L-glutamate and 100 μM glycine in pH 6.8 buffer. The percent current at pH 6.8 was then determined compared to the current at pH 7.6 (defined as 100%).

Zn²⁺ dose inhibition studies: Oocytes expressing recombinant human glutamate receptors were perfused with recording solution containing (in mM): NaCl (90), KCl (1.0), BaCl₂ (0.5), Tricine (10), and HEPES (10) adjusted to pH 7.3 (at 23 degrees C) with NaOH. The oocyte membrane potential was clamped at -20 mV. After a steady baseline is obtained, oocytes were maximally activated with 50 μM L-glutamate and 50 μM glycine, and then in the continuous presence of maximal glutamate and glycine, were perfused with increasing concentrations of Zn²⁺ (1, 3, 10, 30, 100, and 300 nM). . Results at each Zn²⁺ concentration are normalized to the maximum receptor activation levels without Zn²⁺ (defined as 100%) and IC₅₀ values obtained by fitting concentration-inhibition data with Equation 2 (below).

β-Lactamase Assay: HEK cells were plated in 96-well plates and transiently transfected with cDNA encoding GluN2A-WT and β-lac-GluN1-WT or β-lac-GluN1-C744Y. Eight wells were transfected with surface and total expression activities measured in 4 wells each 24 hr post transfection. The ratio of surface (unlysed cells) to total (lysed cells) β-lactamase expression was measured for the β-lac-GluN1-C744Y and compared to β-lac-GluN1-WT. See PMID 27839871 for further information.

Equation 1: Response = 100 / ((1 + EC₅₀ / [agonist])^{nH}) where EC₅₀ is the agonist concentration that elicited the half maximal response, and nH is the Hill slope.

Equation 2: Response = (100 - minimum) / (1 + ([concentration] / IC₅₀)^{nH}) + minimum where minimum is the residual percent response in saturating concentration (constrained to ≥ 0) of the experimental compounds, IC₅₀ is the concentration of inhibitor that causes half maximal inhibition, and nH is the Hill slope.

Statistical comparisons: For analysis of the IC₅₀ or EC₅₀ results, the log values of the IC₅₀'s or EC₅₀'s were used for comparison. If the 95% confidence intervals of WT and variant results for each assay do not overlap, a fold effect was then calculated with positive and negative fold values indicating increased or decreased effect on receptor activity, respectively, for that assay measurement.

b. RESULTS

Measurement	WT Mean	95% CI	n	C744Y Mean	95% CI	n	Fold Effect on NMDAR ^C	Overlap CI
Glutamate EC ₅₀ , μM	4.0	(3.6, 4.5)	12	1.1	(0.9, 1.3)	12	3.8	No
Glycine, EC ₅₀ , μM	1.3	(1.1, 1.5)	10	0.7	(0.61, 0.86)	12	1.8	No
Mg ²⁺ , IC ₅₀ , μM	17	(13, 21)	10	29	(21, 38)	12	NE	Yes
Proton, % ^A	44	(40, 49)	12	74	(68, 81)	12	1.7	No
Zinc, IC ₅₀ , nM	12	(6.8, 21.9)	10	16	(9.7, 27)	12	NE	Yes
Zinc, % residual (Ymin) ^B	28	(18, 37)	10	52	(42, 63)	12	1.9	No
Surface/Total Expression %WT	100	(78,122)	4	68	(58,77)	4	-1.4	No
Total Expression %WT	100	(84,116)	4	150	(133,166)	4	1.5	No

Measurement	GluN1-WT/GluN2A-WT Mean	95% CI	n	GluN1-A653T/GluN2A-WT Mean	95% CI	n	Fold Effect on NMDAR ^C
Glutamate EC ₅₀ , μM	3.2	(2.9,	15	0.12	(0.10, 0.15)	14	26.4

		3.5)					
Glycine, EC₅₀, μM	1.1	(0.9, 1.2)	15	0.024	(0.019, 0.032)	11	44.6
Mg²⁺, IC₅₀, μM	24	(18, 32)	12	23	(17, 31)	12	NE
Proton, %^A	46	(41, 50)	12	88	(85, 91)	11	1.9
Zinc, IC₅₀, nM	6.5	(5.5, 7.7)	12	46	(32, 66)	12	7.1
Zinc, % residual (Ymin)^B	28	(24, 32)	12	67	(57, 75)	12	2.4
Surface/Total Expression %WT	100	(92,108)	4	111	(95,127)	4	NE
Total Expression %WT	100	(95,105)	4	126	(111,141)	4	1.2

Measurement	GluN1-WT/GluN2B-WT Mean	95% CI	n	GluN1-WT/GluN2B-M818T Mean ^D	95% CI	n	Fold Effect on NMDAR ^C
Glutamate EC₅₀, μM	1.0	(0.9, 1.2)	19	0.42	(0.30, 0.58)	19	2.5
Glycine, EC₅₀, μM	0.29	(0.26, 0.33)	20	0.13	(0.097, 0.199)	17	2.2
Mg²⁺, IC₅₀, μM	29	(19, 42)	26	22	(14, 37)	28	NE
Proton, %^A	14	(11, 16)	12	37	(27, 47)	14	2.7
Zinc, IC₅₀, nM	not done	-	-	not done	-	-	-
Zinc, % residual (Ymin)^B	not done	-	-	not done	-	-	-
Surface/Total Expression %WT	not done	-	-	not done	-	-	-
Total Expression %WT	not done	-	-	not done	-	-	-

A: % current remaining measured at pH 6.8 compared to pH 7.6 at maximal L-glutamate and glycine activation

B: Current remaining after maximum inhibition by zinc, i.e., the residual current remaining.

C: Fold effect only calculated if 95% CI's do not overlap. Positive and negative fold effects represent gain of function or loss of function effects, respectively, for the parameter measured. NE = no effect.

n= the number of oocytes evaluated for the measured endpoint; CI = confidence interval.

D: Results for GluN2B-M818T reported here are new data and are in line with results reported previously (Platzer et al., J Med Genet 2017;54:460–70).

4. Neuropathological and immunohistochemical studies

a. Morphological studies

A complete autopsy was performed in the two fetuses (individuals 3 and 4) and one neonate (individual 8) following standardized protocols. Fetal biometric data were evaluated according to Guilhard-Costa et al. (2002). The brains were fixed in a 10% formalin-zinc buffer solution for at least one month. Brain growth and macroscopic assessment of brain maturation including gyration were evaluated according to the criteria of Guilhard-Costa and Larroche and the atlas of Feess-Higgins and Larroche (1990, 1987). Eight-micrometer sections obtained from paraffin-embedded tissues were stained using Haematoxylin-Eosin. Immunohistochemical procedures included a microwave pre-treatment protocol to aid antigen retrieval (pre-treatment CC1 kit, Ventana Medical Systems Inc, Tucson AZ). Incubations with the primary antibodies listed in supplementary Table 1 were performed for 32 or 44 minutes at room temperature using the Ventana Benchmark XT system. After incubation, slides were processed by means of the Ultraview Universal DAB detection kit (Ventana). A comparative semi-quantitative analysis of immunolabellings in the germinative and intermediate zones as well as in the different layers of the frontal cortex of affected and control patients was assessed and evaluated as follows: 0: no cell labelled; +: very few cells labelled; ++: moderate density of immunolabelled cells and +++: high density of immunolabelled cells.

b.

Supplementary Table 6: Antibodies used for the study				
Neural stem cells and progenitors				
Antisera	Cells	Company	Dilution	target
Ki67	Proliferating cells	Agilent	1 :100	Cell cycle related protein
PAX6	Neuroepithelium vRGC, oRGC	Protein Tech group	1 :50	Stem cell transcription factor
SOX2	vRGC, oRGC	Abcam	1 :150	Stem cell self-renewal transcription factor
Ganglionic eminence and cortical interneurons				
GABA	Interneurons	Invitrogen	1:100	Neurotransmitter
Calretinin	Cortical interneurons	Life technology	1:100	Calcium binding protein Cortical interneurons
Post-mitotic neurons and layer markers				
MAP2	Migrating neurons Layers III and V	Sigma Aldrich	1:100	Brain microtubule-associated protein
SATB2	Layers II-IV	Abcam	1:20	Special AT-rich sequence- binding protein
CTIP2	Layers V-VI	Abcam	1:100	COUP-TF-interacting protein 2C2H2 zinc finger transcription factor
vRGC: ventricular radial glial cells; oRGC: outer radial glial cells;				

c.

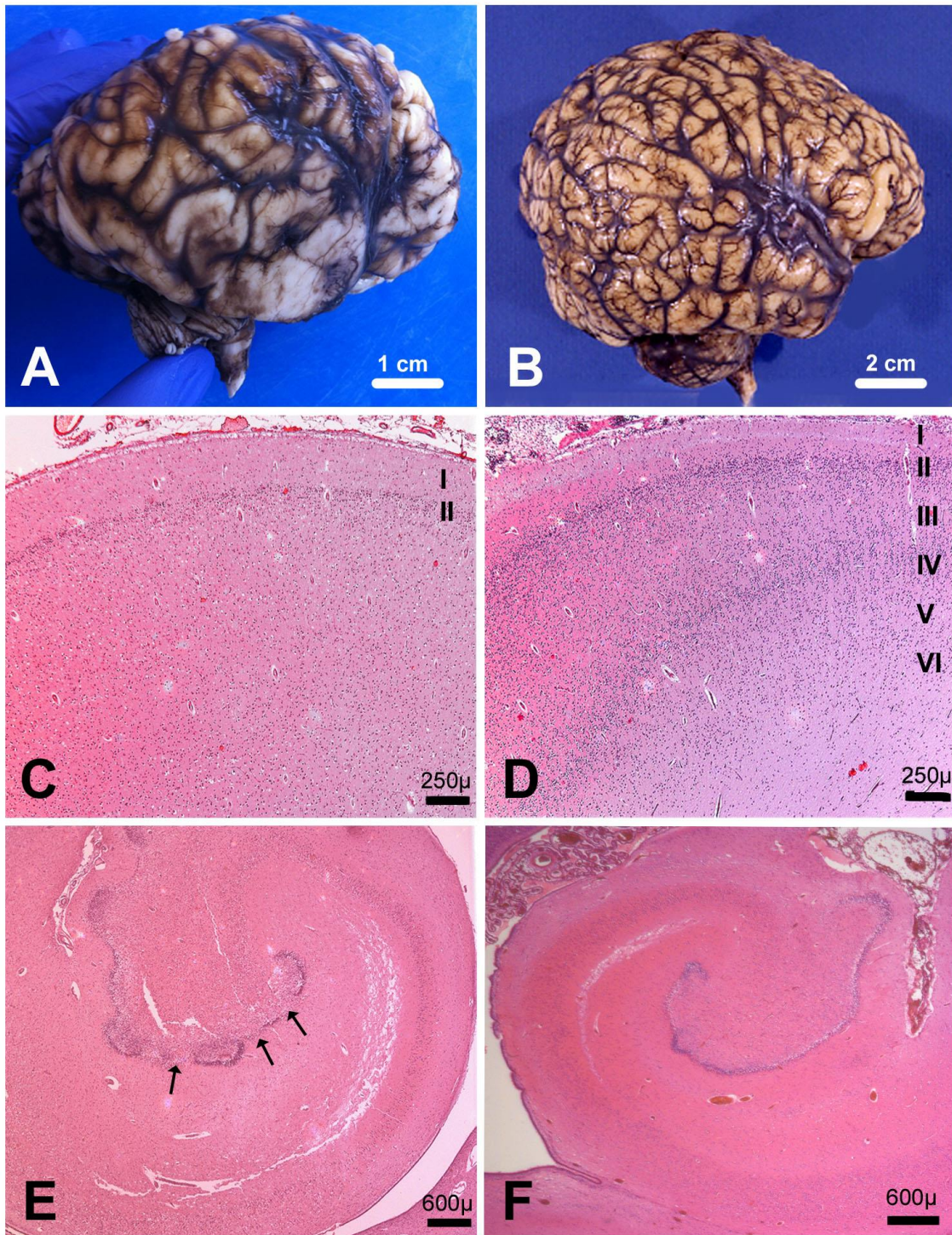
Supplementary Table 7: comparative semi-quantitative analysis of immunolabelling in the germinative and intermediate zones as well as in the different layers of the frontal cortex of affected and control patients

Antibodies	Foetus 1	Control	Foetus 2	Control	Patient 3	Control
	25 WG	25 WG	30 WG	30 WG	38 WG, dead at postnatal day 6	39 WG
PAX6	++ LGE	+++ LGE	0	0	0	0
SOX2	++ LGE	+++ LGE	++ LGE + SVZ	+++ SVZ +++ LGE	NA	++ VZ
Ki67	+ LGE	++ LGE	+++ LGE + SVZ	++ LGE +++ OSVZ	0	0
GABA	0 LGE + IZ + under the CP	+++ LGE +++ VZ, SVZ, ++ CP	+ LGE and SVZ + Superficial micropolygyric CP	++ diffuse CP	+ in layer II and III	++ all layers
Calretinin	0 LGE and VZ + Layer I (Cajal Retzius cells)	+ IZ + VZ + LGE	+ LGE + superficial micropolygyric CP + IZ	+ VZ + LGE ++ Layers II, III and V	Fibre network layer I + interneurons layer II	++ layers II and III

	0 in micropolygyric CP		+++ nodules			
	Dispersed in nodules					
MAP2	Periventricular nodules + Migrating neurons in IZ 0 CP	+++ VZ Layers III and V	+ micropolygyric CP Dysmorphic neurons	++ layer II and III +++ layer V	+ Immature neurons	++ layers III and V
SATB2	Immature neurons in layer II	+ VZ and LGE ++ IZ +++ diffuse CP	0	Layers II-IV +++ in layer II	0	Layers II-IV, +++ in layer II
CTIP2	0	+++ VZ and LGE +++ prospective layer V	0	++ layer V	0	++ layers V and VI

WG: weeks of gestation; VZ: germinative zone of the dorsal telencephalon; SVZ subventricular zone; LGE: lateral ganglionic eminences; IZ: intermediate zone; CP: cortical plate

d. Supplementary figure 1: Main brain macroscopic and histological findings of individual 8



A) Macroscopic view of right side of the neonate brain displaying delayed gyration with no tertiary gyri, broadened sulci and frontal lobe hypoplasia,

B) compared to an age matched control brain, where the tertiary sulcation is in place.

C) Histological view of the temporal cortex in which neuron depletion and dyslamination are observed underneath layer II [H&E, OM x 50],

D) compared with the six-layered cortex of an age-matched control temporal cortex [same OM].

E) Histological view of the hippocampus showing an irregular and fragmented dentate nucleus (arrows), contrasting with a preserved pyramidal cell layer [H&E, OM x 50],

F) compared with a normal hippocampus at the same age [H&E, OM x 50].